Natural Resources Canada | Ressources naturelles Canada

GEOLOGICAL SURVEY OF CANADA
OPEN FILE 7698

Geo-Mapping Frontiers' Chantrey project: bedrock geology and multidisciplinary supporting data of a 550 kilometre transect across the Thelon tectonic zone, Queen Maud block, and adjacent Rae craton

R.G. Berman, L. Nadeau, J.A. Percival, J. Harris, É. Girard, J.B. Whalen, W.J. Davis, D. Kellett, C.W. Jefferson, A. Camacho, K. Bethune

2015

Canada

GEOLOGICAL SURVEY OF CANADA
OPEN FILE 7698

Geo-Mapping Frontiers' Chantrey project: bedrock geology and multidisciplinary supporting data of a 550 kilometre transect across the Thelon tectonic zone, Queen Maud block, and adjacent Rae craton

R.G. Berman[1], L. Nadeau[2], J.A. Percival[1], J. Harris[1], É. Girard[2], J.B. Whalen[1], W.J. Davis[1], D. Kellett[1], C.W. Jefferson[1], A. Camacho[3], K. Bethune[4]

[1]Geological Survey of Canada, 601 Booth St., Ottawa, Ontario
[2]Ressources Naturelles Canada, 490 Rue de la Couronne, Québec, Québec
[3]Dept. of Geological Sciences, University of Manitoba, Winnipeg, Manitoba
[4]Dept. of Geology, University of Regina, 3737 Wascana Parkway, Regina, Saskatchewan

2015

doi:10.4095/296202

This publication is available for free download through GEOSCAN (http://geoscan.nrcan.gc.ca/).

Recommended citation
Berman, R.G., Nadeau, L., Percival, J.A., Harris, J., Girard, É., Whalen, J.B., Davis, W.J., Kellett, D., Jefferson, C.W., Camacho, A., and Bethune, K. 2015. Geo-Mapping Frontiers' Chantrey project: bedrock geology and multidisciplinary supporting data of a 550 kilometre transect across the Thelon tectonic zone, Queen Maud block, and adjacent Rae craton; Geological Survey of Canada, Open File 7698, 1 zip file. doi:10.4095/296202

Publications in this series have not been edited; they are released as submitted by the author.

TABLE OF CONTENTS

Introduction 1
Regional Geological Setting 2
Methods 7
    Fieldwork 7
    Nd tracer isotopes 7
    Geochemistry 7
    U-Pb SHRIMP monazite 9
    Thermobarometric data 9
    ^{40}Ar-^{39}Ar geochronology… 9
Results 11
    Fieldwork 11
    Nd isotopic data 15
    Geochemistry 17
    U-Pb SHRIMP monazite 21
    Thermobarometric data 23
    ^{40}Ar-^{39}Ar geochronology… 24
Discussion 28
Acknowledgements 29
References 30

LIST OF FIGURES

1. Regional geologic setting showing location of Chantrey project 1
2. Aeromagnetic map of Chantrey area showing regional U-Pb zircon ages 3
3. Simplified geological map of the Chantrey area 4
4. Simplified geological map of the Chantrey area with 2012 station locations 11
5. Simplified geological map of the Chantrey area with Nd model ages 16
6. Normative Q' vs ANOR plutonic rock classification diagram 18
7. SiO_2 vs. K_2O diagram 19
8a. Fe* vs. SiO_2 diagram 20
8b. MALI vs. SiO_2 diagram 20
9. Shad plot of aluminum saturation index versus alkali saturation index 21
10. Rb versus Y+Nb diagram 21
11. Simplified geological map with metamorphic monazite and ^{40}Ar/^{39}Ar ages 25
12a. ^{40}Ar-^{39}Ar age results for samples L-018b and L-029a 26
12b. ^{40}Ar-^{39}Ar age results for samples 12PBA-004a and 12PBA-014a 27

LIST OF TABLES

1. Summary of samples with geochronological and/or geochemical data 12
2. Summary of interpreted U-Pb monazite ages and related textures 22
3. Thermobarometric results and associated mineral compositions 24
4. Summary of interpreted ^{40}Ar-^{39}Ar ages 26

Appendices (Digital form only)
The Readme file provides the complete list of files and sub-directories containing the datasets:

1. Summary of samples with geochronological and/or geochemical data
2. Nd isotopic data
3a. Whole rock major element geochemistry (Quebec)
3b. Whole rock trace element geochemistry (Quebec)
3c. Whole rock major and trace element geochemistry (Actlab)
4a. Assay geochemistry (Actlab)
4b. Assay geochemistry (Acme)
5a. SHRIMP U-Pb monazite data – IP692
5b. SHRIMP U-Pb monazite data – IP694
6. SEM images of monazite textures
7a-d. ^{40}Ar-^{39}Ar results 12PBA-004
7b. ^{40}Ar-^{39}Ar results, 12PBA-014
7c. ^{40}Ar-^{39}Ar results, 12NKL-029
7d. ^{40}Ar-^{39}Ar results, 12NKL-018b

Introduction

As part of the Geo-mapping for Energy and Minerals (GEM) program, the Geo-mapping Frontiers project was initiated in 2011 in order to improve geological understanding and help evaluate resource potential of some of the most remote and poorly understood regions of Canada's north. One of the regions targeted was the Chantrey area (Fig. 1), western Nunavut, which includes parts of NTS 1:1 000 000 sheets 76, 66, and 56 (Figs. 2, 3). It overlaps two protected regions: Queen Maud Gulf Migratory Bird Sanctuary and Thelon Game Sanctuary (Figs. 2, 3).

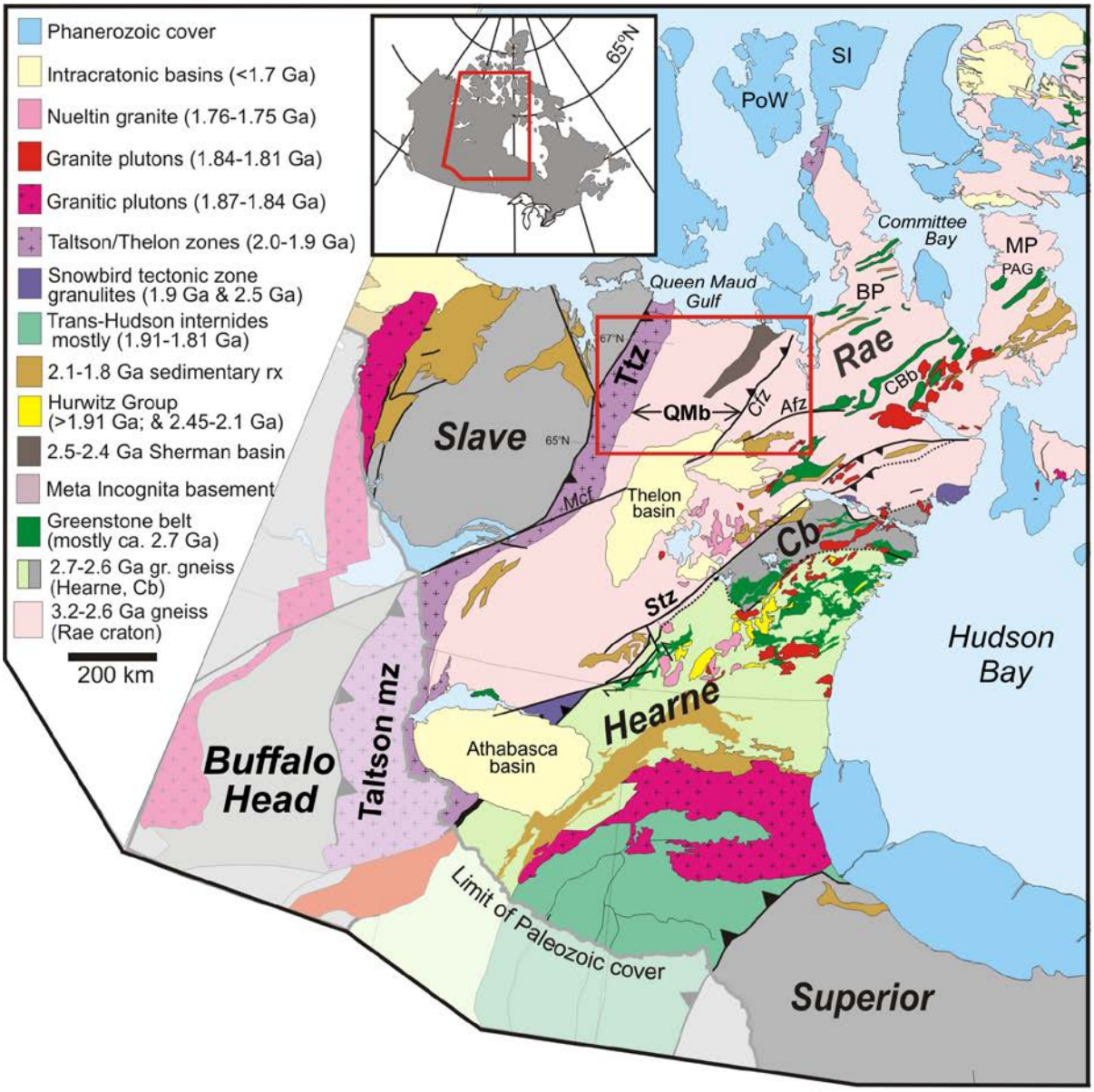

Figure 1: Regional geological map of northwest Laurentia. Area of Figures 2-3 highlighted by red box. Abbreviations:, Afz = Amer fault zone; BP = Boothia Peninsula; Cb = Chesterfield block; CBb = Committee Bay belt; Cfz = Chantrey fault zone; Mcf = McDonald fault; MP = Melville Peninsula; QMb = Queen Maud block; PAG = Prince Albert Group; Stz = Snowbird tectonic zone; Ttz = Thelon tectonic zone.

Major components of work in this region include:

- two high-resolution aeromagnetic surveys (Garry Lake and Pelly Lake; Natural Resources Canada, 2013),
- a remote predictive bedrock map and compilation of legacy data stemming from helicopter surveys in the 1950s and 1960s (Harris et al., 2013),
- U-Pb zircon geochronology of eight samples selected from the GSC's archival collection (Davis et al., 2013),
- a regional stream sediment, heavy mineral and water geochemical survey based on 244 sites spanning much of the Thelon tectonic zone, within the Duggan and Overby Lake map sheets (NTS 76H and 76I; McCurdy et al., 2013)
- surficial geology field observations together with geochemical, heavy mineral, and lithological clast analyses of glacial sediment samples collected from 79 stations in 2012 along a 500-km long, roughly east-west transect (McMartin et al., 2013) (Figs. 2, 3)
- U-Pb zircon geochronology for 16 bedrock samples across this transect (Davis et al., 2014).

This report and the associated digital GIS database present primary field observations made in July, 2012 during helicopter-assisted, targeted field work along the above 500-km long transect (Figs. 2, 3). Also included are laboratory data for selected samples collected along this transect, including whole rock geochemical data, Sm-Nd isotopic data, U-Pb monazite data, ^{40}Ar-^{39}Ar data, and thermobarometric data.

Regional Geologic Setting

Aeromagnetic data (Natural Resources Canada, 2013) combined with several geochronological transects (Schultz et al., 2007; Tersmette, 2012; Davis et al., 2013, 2014) provide first order division of the region into distinct crustal domains (Figs. 2, 3) which are described below from west to east.

Thelon tectonic zone (Ttz)

The Thelon tectonic zone (Ttz) comprises a series of pronounced, ~500 km long, NNE-striking magnetic anomalies that separate the Slave craton from the Queen Maud block (Fig. 1, 2). Similarities in magnetic fabrics and plutonic rock ages led to the suggestion that the Ttz is correlative with the Taltson magmatic zone south of the MacDonald fault (Hoffman, 1988; Fig. 1). The Thelon tectonic zone has been postulated to represent a ca. 2.0 Ga continental arc built on the western flank of Rae craton and subsequently intensely deformed during ca. 1.97 – 1.90 Ga collision of the Slave craton (Hoffman, 1988). An alternative model based on geochemical data for Taltson plutonic rocks proposes that the Taltson-Thelon zone formed as an intracontinental mountain belt far removed from an active plate boundary (Chacko et al., 2000; Schultz et al., 2007).

The Ttz has been investigated in three widely separated areas:

- a southern region between the MacDonald fault and 65°N (Henderson et al., 1987; van Breemen et al, 1987a, van Breemen and Henderson, 1988; James et al., 1988, Henderson and van Breemen, 1992) and also including a small part of the Great Slave shear zone further west (van Breemen et al., 1990),
- a central region between 65°N and 67°N (Frith, 1982a, b; Thompson, 1986; Thompson et al., 1986; van Breemen et al., 1987b; Frith and van Breemen, 1990; Davis et al., 2013, 2014) that in part coincides with the western part of the Chantrey project area (Figs. 2, 3),
- the westernmost sample (QM-6) of a coastal transect along Queen Maud Gulf at ~68°N (Tersmette, 2012; Fig. 2).

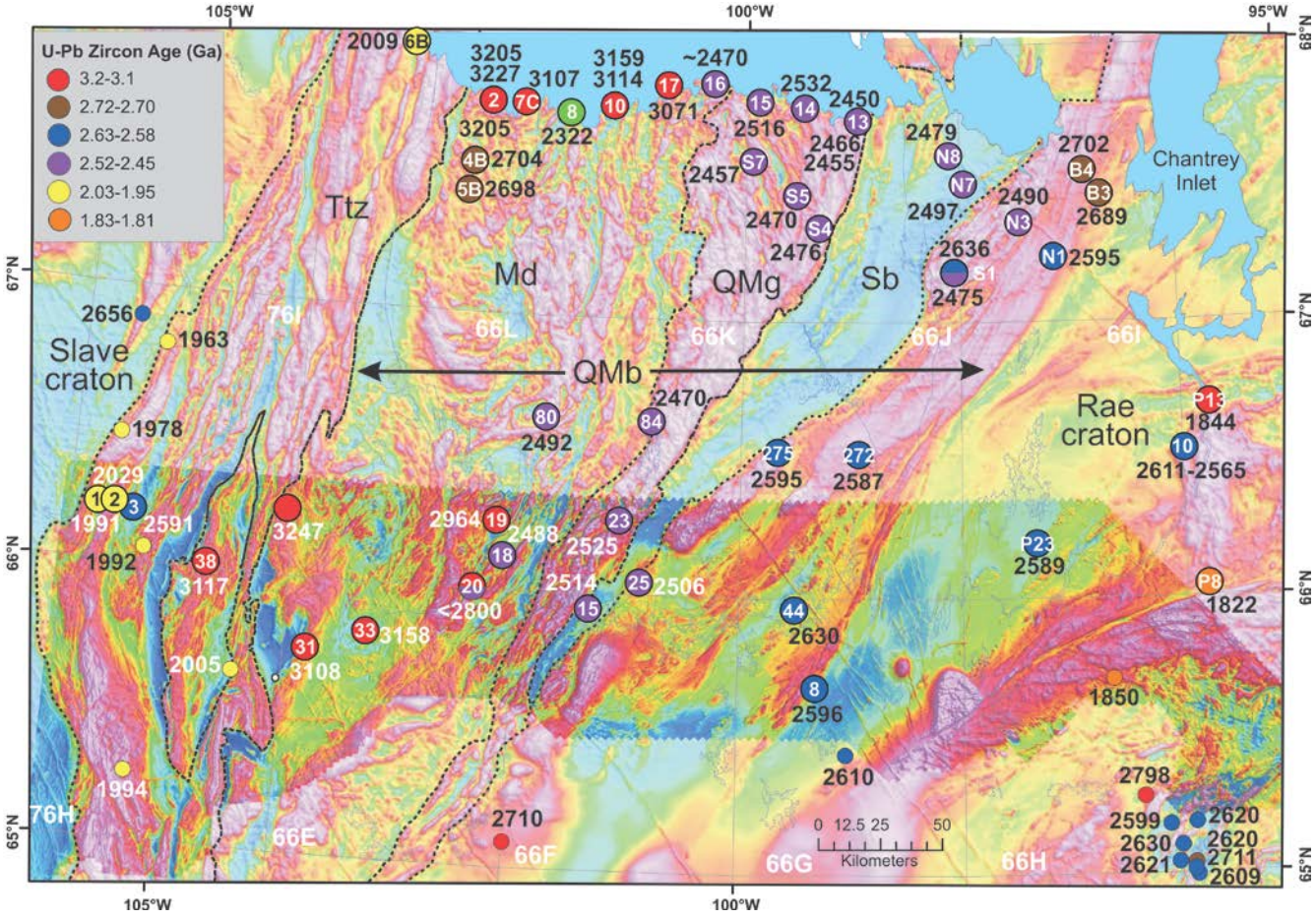

Figure 2: Aeromagnetic map showing interpreted boundaries (dashed curves) between geologic domains within the Chantrey project region (modified from Berman et al., 2013a), along with locations establishing regional geochronological control. Numbers inside symbols refer to abbreviated sample numbers from the main sources of data (Schultz et al., 2007; Tersmette 2012; Davis et al., 2013, 2014).

The region as a whole is dominated by granitic to tonalitic metaplutonic rocks that include homogenous granitoid, migmatitic gneiss, and layered migmatite. In widespread granulite-facies regions, clinopyroxene and/or orthopyroxene occur in addition to hornblende and biotite. Supracrustal rocks occur as long, narrow lenses or belts (>10 km) and include pelitic, psammitic, calc-silicate, and mafic metavolcanic rocks. The

pronounced, north to NNE-striking aeromagnetic fabric of the Ttz reflects strong Paleoproterozoic deformation that also produced high strain zones in the eastern Slave craton (Thompson et al., 1986).

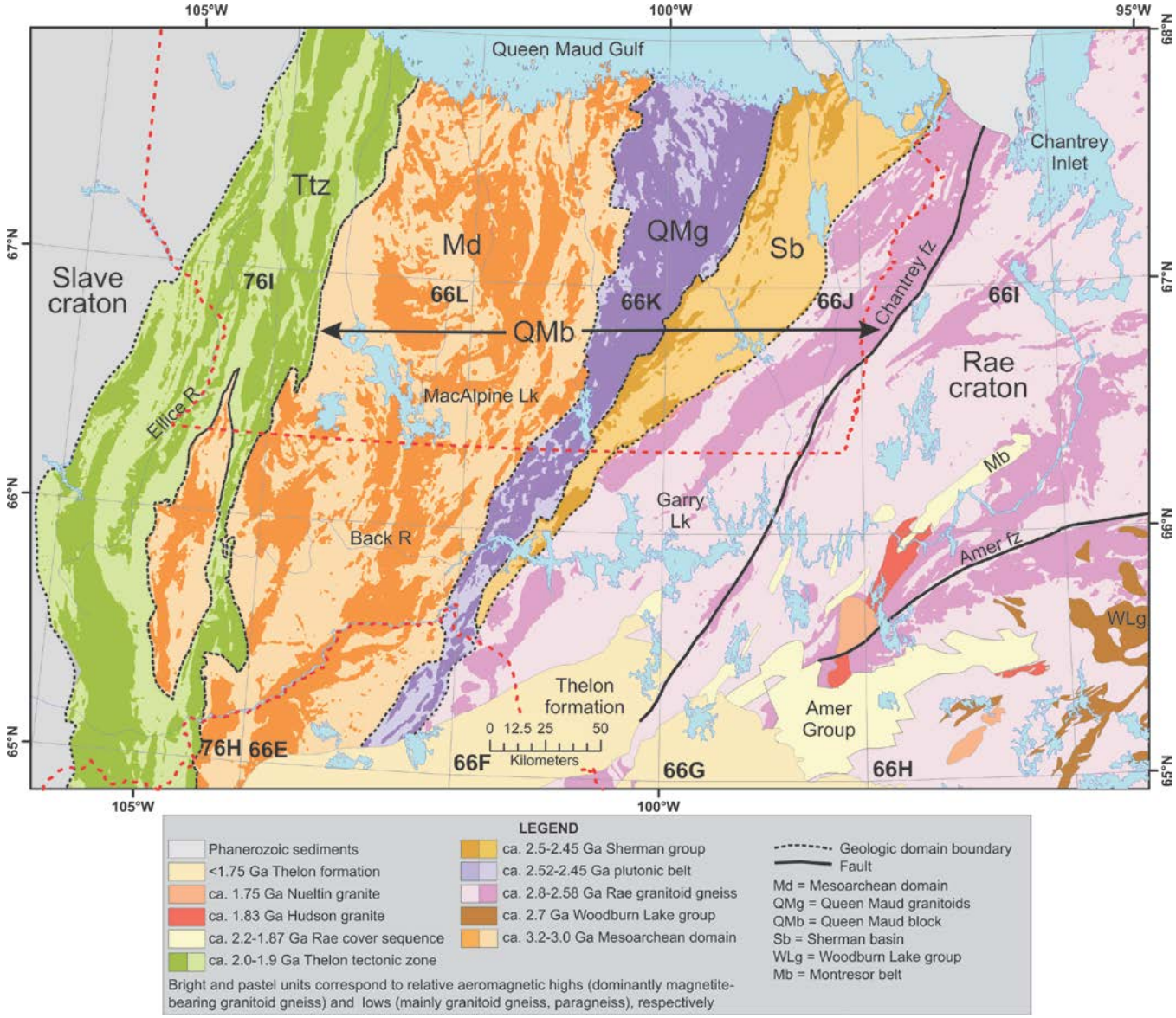

Figure 3: Interpreted geologic domains based on aeromagnetic and geochronological data (modified from Berman et al., 2013a). Red dotted curves are boundaries of the Queen Maud Gulf Migratory Bird Sanctuary (north) and Thelon Wildlife Sanctuary (south).

Geochronological data in each area reveal high-grade metamorphism and/or granitoid plutonism at ca. 2000 Ma. In the southern region, a 1997 ± 2 Ma zircon fraction (fraction 2a; van Breemen et al., 1987a) provides a minimum age of igneous crystallization for a mylonitized granodioritic granulite gneiss. Metamorphism was dated at 2000 ± 10 Ma from metamorphic zircon in well-foliated Hbl-Grt paragneiss (Henderson and van Breemen, 1992). In the central region, plutonism is present in the form of 2029 ± 4 Ma Cpx-

bearing quartz monzonite gneiss (L2 in Fig. 2; Davis et al., 2014), Hbl-Mt granodiorite gneiss at 2005 ± 5 Ma (Davis et al., 2013), K-feldspar megacrystic granite at 1994 +6/-4 Ma (Frith and van Breemen, 1990), and Opx-Bt monzogranite at 1991 ± 4 Ma (L1 in Fig 2; Davis et al., 2014). In the northern transect, strongly magnetic, Cpx-Bt-Hbl granodiorite gneiss is dated at 2009 ± 17 Ma (QM-6, Tersmette, 2012).

Younger plutonism has also been documented in the Ttz. In the southern region, poorly foliated, biotite granite crystallized at 1978 ± 5 Ma (van Breemen et al., 1990), and strongly deformed Cpx granite at 1957 +9/-5 (James et al., 1988), Hbl granite at 1950 ± 5 Ma (van Breemen and Henderson, 1988), and granodiorite at 1920 ± 4 Ma (van Breemen et al, 1987a). In the central region, massive to weakly foliated clinopyroxene granodiorite crystallized at 1978 ± 2 Ma (Frith and van Breemen, 1990), and moderately foliated K-feldspar granodiorite at 1963 +4/-3 (van Breemen et al., 1987b). Syntectonic, S-type granite was emplaced at 1908 ± 2 Ma (monazite; van Breemen et al., 1987b) during high-grade metamorphism dated at 1906 ± 2 Ma (Roddick and van Breemen, 1994) and between 1908 Ma – 1902 Ma at a number of locations in the Ttz and adjacent Mesoarchean domain (Davis et al., 2013, 2014).

Queen Maud block (QMb)

The Queen Maud block was distinguished on the basis of its high metamorphic grade relative to proximal areas (Committee and Armit blocks) of the northern Churchill province. Originally defined by Heywood and Schau (1978) to extend north of the MacDonald fault to Queen Maud Gulf, and east of the Ttz to the Chantrey fault zone, Schultz et al. (2007) suggested that the eastern boundary of the block shift west to coincide with a prominent magnetic lineament interpreted to reflect the eastern limit of a newly discovered ca. 2.5 Ga plutonic belt (QMg on Fig. 2). In this report we retain the original definition as a geographic description (e.g. Figs. 2, 3).

The geology of the QMb is not well established, with no systematic mapping subsequent to the initial helicopter surveys in the 1950's and 1960's (Heywood, 1961; Bostock et al., 1963). Sm-Nd isotopic analyses of samples across the southwestern and central QMb identified significant 3.6-3.1 Ga crustal signatures (Thériault et al., 1994). Recent U-Pb geochronological data (Tersmette, 2012; Davis et al., 2013, 2014) demonstrate a broad extent of Mesoarchean crust between the Thelon basin and Queen Maud Gulf (Fig. 2). The westernmost extent of Mesoarchean crust is provisionally interpreted on the basis of aeromagnetic characteristics to be isolated by a belt of Thelon-aged plutonic rocks. Mesoarchean crust is flanked on its east by orthopyroxene-magnetite-bearing, 2.52–2.45 Ga granitoid rocks (Schultz et al., 2007; Tersmette, 2012; Davis et al., 2013, 2014), referred to as the Queen Maud granitoid belt (QMg, Schultz et al., 2007), that correspond to a pronounced NNE-striking magnetic high (Fig. 2). East of this plutonic belt is a strong magnetic low coinciding with the Sherman supracrustal group (Schultz et al., 2007; Sb on Fig. 2). This group is dominated by ca. 2.5-2.45 Ga

provenance, and is considered to have been deposited in a continental rift after 2.45 Ga (youngest detrital zircon) and before ca. 2.39 Ga, the time of metamorphic monazite growth (Schultz et al., 2007).

Hoffman (1988) interpreted the Queen Maud block as the exhumed part of a tectonic plateau developed behind the Thelon tectonic zone as a consequence of Himalayan-style, ca. 1.97 Ga collision of the Slave and Rae cratons. This model was challenged by Schultz et al. (2007) and Tersmette (2012) who identified a significant 2.5–2.3 Ga plutono-metamorphic history in the area, indicating that much of the high-grade metamorphism predates the Thelon orogeny and instead forms part of the Arrowsmith orogen that developed on the western margin of the Rae (Berman et al., 2005; 2013b).

Rae craton

The Rae craton west of Hudson Bay is dominated by Neoarchean plutonic and supracrustal rocks with lesser Mesoarchean basement gneiss. With the notable exception of the ca. 2.97 Ga Prince Albert group on Melville Peninsula (Frisch, 1983; Wodicka et al., 2011), supracrustal belts are dominantly Neoarchean and include quartzite-komatiite supracrustal rocks of the 2.72-2.68 Ga Committee Bay belt (Skulski et al., 2003; MacHattie, 2008; Sanborn-Barrie et al., 2014) and Woodburn Lake groups (Ashton, 1988; Fraser, 1988; Zaleski et al, 2000; Pehrsson et al., 2013). The most voluminous component of the extensive granitoid domain is a suite of ca. 2.62 – 2.58 Ga plutons of dominantly monzogranitic composition (Skulski et al., 2003; Hinchey et al., 2011 and references therein; Sanborn-Barrie et al., 2014) which extend as far west as the Sherman basin and QMG (Figs. 2, 3; Davis et al., 2013, 2014). Metamorphosed remnants of what is thought to have been an extensive ca. 2.1–1.9 Ga Palaeoproterozoic sedimentary cover include the Amer, Ketyet River, Montressor, Chantrey, and Penrhyn groups (Fig. 1; Rainbird et al., 2010 and references within). Generally post-tectonic plutonic suites include the ca. 1.85–1.81 Ga Hudson granites (Fig. 1), interpreted as orogenic lower- to mid-crustal melts (Peterson et al., 2002), and the ca. 1.76–1.75 Ga Nueltin granites (Fig. 1), interpreted as upper crustal melts triggered by a mafic underplate (Peterson et al., 2002). A northeast-striking foliation is characteristic of the region and has been demonstrated in the Committee Bay belt and southern Boothia Peninsula to be Paleoproterozoic in age (Berman et al., 2005; 2008; 2010). Indentation of the Slave craton (Henderson et al., 1990) is considered to have driven latest dextral movement in the Chantrey (Hoffman, 1989; Tella, 1994; Frisch, 2000) and Amer (Tella and Heywood, 1978; Tella, 1994) fault zones.

Methods

A. Field data

Field data and samples (Appendix 1 contains a subset with geochemical and/or geochronological data) were collected between July 15 and July 25, 2012. In the text and figures, sample collection numbers have been abbreviated by either omitting the prefix "12NK-", or abbreviating "12JP-" as "J" and "12PBA-" as "P". Helicopter access to the eastern region was from the town of Baker Lake and to the western region from the Mianiqsijit Project's Sahara field camp, located approximately 160 km northwest of Baker Lake.

B. Neodymium isotopes

Neodymium isotopic analyses (Appendix 2) were performed at the Isotope Geochemistry and Geochronology Research Centre, Department of Earth Sciences, Carleton University. Samples were dissolved in 0.26N HCl and loaded onto Eichrom Ln Resin chromatographic columns containing Teflon powder coated with HDEHP [di(2-ethylhexyl) orthophosphoric acid] (Richard et al., 1976). Nd was eluted using 0.26N HCl, followed by Sm in 0.5N HCl. Total procedural blanks for Nd are < 50 picograms; < 6 picograms for Sm. Samples were spiked with a mixed ^{148}Nd-^{149}Sm spike prior to dissolution. Concentrations are precise to ± 1%, while ^{147}Sm/^{144}Nd ratios are reproducible to 0.5%. Samples were loaded with H_3PO_4 on one side of a Re double filament, and run at temperatures of 1700-1800 ^{o}C. Isotope ratios are normalized to ^{146}Nd/^{144}Nd = 0.72190. Analyses of the USGS standard BCR-1 yield Nd = 29.02 ppm, Sm = 6.68 ppm, and ^{143}Nd/^{144}Nd = 0.512668 +/- 20 (n=4). The international La Jolla standard produced: TRITON: ^{143}Nd/^{144}Nd = 0.511847 +/- 7, n = 26 (Feb 2005 – June 2007). The internal lab Nd standard gave: 0.511818 +/- 8, n = 28 (Feb 2005-June 2007); 0.511819 +/- 10 n = 94 (Feb 2005 – Aug 2009); 0.511823 +/- 12 n = 65 (Oct 10 – July 12).

C. Geochemistry

Geochemical samples typically consisted of ~1.5 – 2.0 kg (depending on rock texture and grain size) of fresh, clean, texturally and mineralogically homogeneous rock fragments (up to 10) selected as representative of a specific lithology. Crosscutting veins, altered fractures and surface alteration were avoided. Fragments were broken on their own outcrop to remove weathering and limit the potential for contamination. Representative hand samples were systematically collected from the same sampling material, but some hand samples are less texturally homogeneous than the fragments screened for geochemistry.

Whole rock major (Appendix 3a) and trace (Appendix 3b) element data for most samples were acquired at GSC Quebec (see Appendix A for preparation and analytical methods). Duplicate analyses of some samples as well as laboratory standards are included in these appendices. During sample preparation, each rock fragment was pressure air cleaned prior to sub-centimeter size steel-plated jaw crushing. The jaw mill was scrubbed (plastic brush), vacuum cleaned and blown with compressed air before use with each sample. Rock chips were

hand-split to pick-out 300-500 g of grain size unsorted fragments for shatter box (Fe-Cr-steel alloy ring mill) pulverization; 50-80 g of pulverized rock pulp was used for chemical analysis. Potential pulverization contaminants consist of Fe, Si, with very small traces (<10 ppm) of Cr, Al, Na, Fe, K, Ca, Mg, Ba, Ce, Sr, and Pb.

Chemical analyses were all made in a single batch at the INRS-ETE laboratory in Quebec City. Samples were analyzed through a combination of inductively coupled plasma mass spectroscopy (ICP-MS) for trace elements, and inductively coupled plasma emission spectroscopy (ICP-ES) for major and some trace elements. Sample decomposition (digestion) was achieved through lithium metaborate fusion and dissolution in dilute nitric acid. Quality assurance / quality control (QA-QC) was assessed for each analytical method according to the precision of the certified standards and duplicate analyses, analytical limitations of the methods for specific elements.

Access to the INRS-ETE laboratories in Quebec City is restricted to analytical staff and controlled by electronic detectors. Equipment that is especially sensitive to contamination (e.g., ICP-MS) is located in a class 10000 clean room. Instruments for metal analysis in geological samples consist of an ICP-MS (Thermo Instruments X7), ICP-AES (Varian 725 (Radial)), and a fluxer (Fluxy, Corporation scientifique Claisse). All acids are of trace-metal grade and solutions are made with >18MΩ cm water. Handling and sample preparation are designed to minimize trace-element contamination. Multi- and single-element calibration standards are made from single-element, certified standards, traceable to NIST, purchased from SCP Science. Five certified reference materials are used: Sarm-1 (Bushveld granite), Sarm-5 (pyroxenite), BCR-2 (basalt Columbia River), BHVO-2 (basalt Hawaiian volcanic observatory) and W2 (diabase).

Once the performance of analytical equipment is tested, generally by analysing the signal given by a solution of known composition, it is calibrated with standard solutions. The calibration curve (7-10 points) is repeated each time that a new series of analyses is initiated. Every 15 samples, blanks (analytical and methodological) are re-analysed as well as duplicates and standards. Furthermore, for each analysis, an internal standard is use to identify possible matrix problems or other problems. Internal standards may be used to correct results. No sample measurements are made if the control solutions give anomalous readings until problems have been clearly identified and resolved. Samples having suspect values are re-analyzed. The INRS-ETE laboratory is a regular participant in inter-laboratory comparative studies organized by the National Water Research Institute of Canada.

Major and trace element data for two samples (P13, P23; Appendix 3c), major element data for 6 samples (L20a, L20c, L4c, L37, J61, P27; Appendix 3c), and assays for two other samples (L20b; J51; Appendix 4a) were analyzed by Activation Laboratories in Ancaster, Ontario. Assays for PBA samples (Appendix 4b) were obtained from Acme Analytical Laboratories, Vancouver, B.C. Crushing method, and analytical techniques and detection limits for each element are reported in Appendices 3c, 4a, and 4b. Details of analytical

methods are available at www.actlab.com and www.acme.com, respectively.

D. Monazite Geochronology

Five rock samples were chosen that contained monazite of a size (>10 µm) suitable for *in situ* SHRIMP analysis, carried out on 3 mm-diameter cores drilled from texturally significant areas of polished thin sections following the methods of Rayner & Stern (2002). A small plug of pre-polished laboratory standard monazite (GSC monazite z3345 & z2908) was included on the mount. Stern and Berman (2000) describe further analytical details. A Pb fractionation correction was applied to the Pb-isotope data in some instances (see Appendix 5 footnotes), the magnitude of which was determined by the analysis of monazite standards z3345 and z2908 whose $^{207}Pb/^{206}Pb$ ages have been determined by isotope dilution methods (Stern and Berman, 2000). The error associated with the mass fractionation correction was added quadratically to the isotopic ratios when weighted mean ages were calculated. Common Pb correction utilized the Pb composition of the surface blank (Stern, 1997). Appendix 6 shows textural locations of some of the analyzed monazite grains.

E. Thermobarometric data

P –T conditions were estimated using the winTWQ software (version 2.35; Berman, 2007) following the methodology summarized by Berman et al. (2005). Unless stated otherwise , chemical variations in Fe/(Fe+Mg) of biotite and cordierite, and X_{An} of plagioclase are less than 2 percent, and P-T values were calculated from nearby rim compositions of ferromagnesian minerals (garnet, biotite, cordierite) separated by quartz and/or plagioclase.

F. ^{40}Ar-^{39}Ar data

Samples were processed for $^{40}Ar/^{39}Ar$ analysis using standard mineral separation techniques, including hand-picking of inclusion-free unaltered hornblende/biotite crystals in the size range 250-500µm. The grains were loaded into an aluminum foil packet, along with several grains of hornblende reference material PP20 (equivalent to HB3gr, 1074 ± 5 Ma 1σ; Jourdan et al., 2006) to act as flux monitor. The packet was arranged radially in an aluminum canister (40×19 mm), Cd-shielded and irradiated for 960 MWH (2-2.5 MW) in medium flux position 8c at the research nuclear reactor of McMaster University (Hamilton, Ontario). Laser $^{40}Ar/^{39}Ar$ step-heating analyses of the irradiated samples were carried out at the Geological Survey of Canada (Ottawa). For step-heating, single-grain aliquots of the sample were loaded into 1.5 mm diameter holes in a copper planchet and stepwise heated under vacuum using a Photon Machines Ltd. Fusion 10.6 55W CO_2 laser equipped with an optical beam-flattening homogenizer lens. The released Ar gas was cleaned over getters for three minutes before isotope analysis using a Nu Noblesse multicollector mass spectrometer; details of data collection

protocols can be found in Kellett and Joyce (2014). Data reduction and age calculations were performed using Mass Spec software version 7.93 (Deino, 2001) and constants outlined in Kellett and Joyce (2014). Neutron flux gradients were evaluated by analyzing multiple PP20 flux monitors and interpolating a fit against calculated J-factor and sample position. The error on the J-factor value is conservatively estimated at ±0.6% (2σ). Blank levels are reported in the data tables.

Multiple aliquots were evaluated to establish reproducibility of apparent age spectra. Reported statistical plateaux (Appendix 7) were defined on the basis of three or more consecutive heating steps that are within error of each other that comprise >50% of the total ^{39}Ar released. Where these criteria were not met, flat segments of the age spectra from individual aliquots were integrated (weighted by analytical error) to calculate apparent ages, and used as the basis for the interpreted ages.

Results

A. Field data

A total of 237 bedrock outcrops were studied along a roughly east-west transect across the area (Fig. 4). All outcrop observations, including structural measurements and photographs, are provided digitally. Geochronological and/or geochemical data were acquired for 41 bedrock samples (Fig. 4) summarized in Table 1. Further details of these samples are provided in Appendix 1.

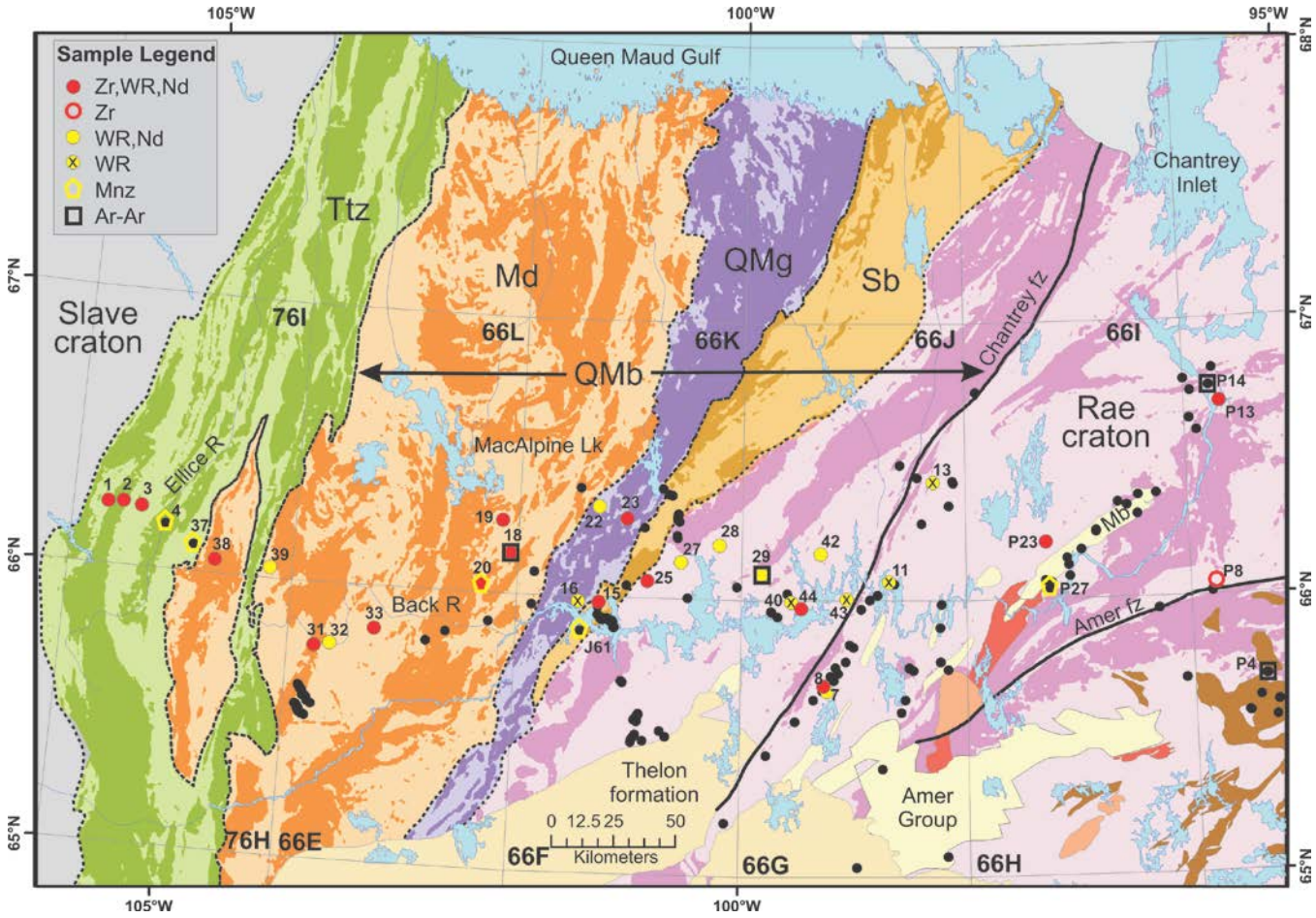

Figure 4. Regional geology of the Chantrey region (see Fig. 3 for legend)). Abbreviations: Mg = Montresor group; QMB = Queen Maud block. Unnumbered black dots show mapping localities whereas labelled symbols show locations of bedrock stations with acquired laboratory results shown in the legend: Zr = U-Pb zircon crystallization age; WR = whole rock major and trace element geochemistry; Nd = Nd-Sm isotopic data; Mnz = U-Pb in situ SHRIMP monazite age; Ar-Ar = ^{40}Ar-^{39}Ar age on hornblende or biotite. Alphanumeric label refers to abbreviated sample number cross-referenced in figures, tables and appendices and in Davis et al. (2014).

Table 1. Summary of sample results

Station	Lithology[1]	Mineral Assemblage[2]	Textures	Zrn Age[4]	Err-or	Mnz Age[5]	Err-or	Nd Age[6]	Ar-Ar Age[7]	Chem istry[8]
12JP-061a	Gt-Sil diatexite	Grt-Bt-Sil-Crd Ap-Mz-Zc-Ilm-Pyrh-Rt	strongly embayed Grt with Sil inclusions & large Kfs porphyroclasts, wrapped by strong foliation defined by qfp shape and Bt and Sil			2504	5			m
12NK-L001a	Foliated Opx-Bt monzogranite	Opx-Bt-Ap-Pyrr-Zc	moderate foliation defined by qfp shape mostly; embayed Opx commonly rimmed by Bt; some Bt rimmed by Chl; some sericite	1991 1927m	4 26			2464		t
12NK-L002a	Foliated, migmatitic Hbl-cpx quartz monzonite gneiss	Bt-Hbl-Cpx-Mt-Ap-Zc	Leucocratic bands have larger, somewhat elongate feldspars and elongate aggregates of recrystallized qfp; no reaction relationships between mafic minerals	2029 1994m	4 13			2504		t
12NK-L003a	Bt-Mt monzogranite gneiss	Bt-Mt-Ap-Ttn-Aln	gneissosity defined by Bt-Mt layers imperfectly separated from leucocratic layers w larger feldspars and elongate aggregates of recrystallized Qtz	2591, 1902m	27 9			2833		t
12NK-L004a	Grt-Sil-Bt metatexite	Grt-Sil-Crd-Bt Pyrr-Ilm-Ap-Mz-Zc	Grt-Sil wrapped by recrystallized qfp bands; Bt mostly post-tectonic; Crd-->Chl			1992 1902	5 5			m
12NK-L007a	Mylonitic Ms monzogranite	Ms-Bt-Ttn-Ap-Zr-Mnz-(Chl)	Kfs-Pl porphyroclasts in fg, partially recrystallized, mylonitic matrix; Ms as cg, primary grains and fg matrix grains; fg Bt is minor component					2997		t
12NK-L008a	Hbl-Bt quartz monzodiorite	Hbl-Bt-Mt-Ttn-Pyrr-Ap-Zc-(Ep-Chl-Ser)	Weakly deformed, plagioclase porphyritic	2596	3			2821		t
12NK-L011a	Ms monzogranite cobble in conglomerate	Ms-Bt-Zr-(Chl-Ser)	undeformed, feldspars altered to sericite							t
12NK-L013a	Well foliated, Bt-Ms Plg porphyritic monzogranite gneiss	Bt-Ms-(Chl-Ep)	Moderately deformed, Pl porphyroclasts in mg matrix of qfp, Bt, Ms; Chl after Bt							t
12NK-L015a	Cpx-Hbl quartz diorite gneiss	Cpx-Hbl-Bt-Opx-Ap-Aln	layers of elongate qfp with disseminated Bt and Cpx-Hbl rich layers, with rare Opx cores; minor Chl rims on Bt	2514	3			2788		t
12NK-L016b	Foliated Opx-Bt quartz diorite	Opx-Bt-Mt-Hbl-Ap-Zc	Abundant pristine Opx, equigranular, some Bt after Mt							t
12NK-L018a	Moderately foliated Bt alkali feldspar granite	Bt-Fl-Ap-Rt-Zc-Aln-Mo-Mt	moderate foliation defined by biotite alignment; rare Kfs up to 1 cm within granoblastic qfp matrix	2488 2378m	5 4			3029		t
12NK-L018b	Quartz gabbro dyke	Cpx-Hbl-(Opx)-Pl-Ilm	Subophitic igneous texture preserved; Hbl rims/grains around Cpx						<1980 h	t
12NK-L019a	Foliated Opx-Bt syenogranite	Opx-Bt-Ilm-Mt-Zc	layers with partially recrystallized, elongate qfp separated from those with scattered Bt and Opx; some Opx --> Bt	2964	7			3218		t

Table 1. Summary of sample results (continued)

Station	Lithology[1]	Mineral Assemblage[2]	Textures	Zrn Age[4]	Error	Mnz Age[5]	Error	Nd Age[6]	Ar-Ar Age[7]	Chemistry[8]
12NK-L020a	Strongly foliated Grt-Bt-Sil diatexite	Grt-Bt-Sil-Sp-Pl-Py-Pyrr-Rt-Zc-Mz-Ap	Anhedral Grt (<6 mm) in part truncates and in part is enveloped by foliation defined by highly attenuated quartz lenses within mostly recrystallized, fg qfp matrix; Sp-Qz intergrowths (after Crd+-Sil?); much Bt is post-tectonic and some from Grt breakdown			2369 2344	8 12			m
12NK-L020c	Strongly foliated S-type alkali feldspar granite	Grt-Bt-Sil-Ilm-Zc-Mz-Ap	Anhedral, elongate Grt (up to 1 cm long) enveloped by Kfs-rich and Qz-rich layers aligned with scattered Bt blades	<2800		2367	5	3223		t
12NK-L022a	Foliated Bt monzogranite	Bt-Mt	Larger feldspars in fg Qtz-rich matrix with sutured grain boundaries					3059		t
12NK-L023a	Foliated Bt-Mt-Opx tonalite	Bt-Mt-Opx-Ilm-Pyrr-Zc	Strong foliation defined by aligned Bt-Mt-Opx and moderate qfp shape; some Opx --> Chl	2525 2426m	4 7			2760		t
12NK-L025a	Strongly foliated Hbl-Bt-Mt monzogranite	Hbl-Mt-Bt-Ttn-Ep-Zc-Pyrr-Ap	Foliation defined by strong qfp shape aligned with Bt and Hbl-Mt aggregates; some Hbl rimmed by Ep and Bt	2506 1937m	3 22			2823		t
12NK-L027a	Foliated Bt-Ttn syenogranite gneiss	Bt-Ttn	Larger feldspars in qfp matrix with sutured grain boundaries					2733		t
12NK-L028a	Foliated Bt-Fl monzogranite	Bt-Fl-Ap-Zc	Subequant Kfs-Pl phenocrysts set in qfp matrix with moderate shape fabric defining foln					2830		t
12NK-L029a	strongly foliated Hbl-Bt-Mt quartz monzonite	Hbl-Bt-Mt-Pyr-Ap-Zc	foliation defined by distinct qfp shape aligned with Hbl and Bt					2802	1863b	t
12NK-L031a	foliated Hbl granodiorite	Hbl-Bt-Ap-Py-Zc	Hbl-rich layers and qfp layers with strong shape fabric and some Pl porphyroclasts	3108 2325m 1908m	58 100 6			3609		t
12NK-L032a	foliated Bt-Mt syenogranite	Bt-Mt-Ilm-Zc	foln defined by Bt; fg recrystallized qfp matrix					2766		t
12NK-L033a	Bt-Hbl tonalite gneiss	Bt-Hbl-Ttn-Py-Ap-Zc-(Ep-Cc)	granoblastic qfp layers with some larger, elongate Pl and Hbl-Bt-rich layers; some Bt rimmed by fg Ep	3158 2342m	42 7			3079		t
12NK-L037a	Strongly foliated Grt-Sil diatexite	Grt-Sil-Ilm-(Bt)-Crd	small (< 1mm), embayed Grt and sil blades within fg, mostly recrystallized qfp matrix; strong foliation defined by alignment of sillimanite and some elongate Grt with attenuated quartz (up to 6:1 ratio); late Bt from Kfs+Ilm			1903 1881	10 13			m
12NK-L038a	Well foliated Opx monzogranite gneiss	Opx-Ilm-Mt-Bt-Ap-Zc	foliation defined mainly by Opx and Ilm aligned with shape of some large qfp grains in mainly recrystallized qfp matrix; some Opx-->Chl	3117, 2379m 1906m	21 22 13			3211		t
12NK-L039a	Strongly foliated Sp-Sil alkali granite gneiss	Sp-Sil-Rt-Ilm-Bt-Zc-	strongly foliated with Fe-rich Sp-Sil bands; only trace of biotite (mostly around Sp)					2594		t
12NK-L040a	undeformed Bt monzogranite	Bt-Zc-Mt?	Pl and lesser Kfs phenocrysts in finer grained matrix with sutured gb's							t
12NK-L042a	Undeformed Hbl-Bt quartz diorite	Hbl-Bt-Ilm?	poikiolitic igneous texture, with late qtz surrounding Pl-Kfs-Bt-Hbl					2763		t

Table 1. Summary of sample results (continued)

Station	Lithology[1]	Mineral Assemblage[2]	Textures	Zrn Age[4]	Error	Mnz Age[5]	Error	Nd Age[6]	Ar-Ar Age[7]	Chemistry[8]
12NK-L043a	Variably deformed Kfs porphyritic syenogranite	Ttn-Mt-Ilm-Ep-Ap-Zc	moderately foliated, with marked grain size reduction and recrystallization along boundaries of Kfs phenos and qfp matrix grains; Pl-->sericite							t
12NK-L044a	feldspar porphyroclastic monzogranite	Ms-Bt-Ep-Ttn-Zc-Py-(Chl)	Kfs-Pl porphyroclasts enveloped by strong foliation defined by fg qfp shape, Bt, and Ms;	2630	3			2854		t
12PBA-004a	Foliated Hbl-Bt tonalite gneiss	Hbl-Bt-Ep-Ap-Ilm?-(Chl)	foliation defined by moderate qfp shape aligned with Hbl and Bt; some alteration of Bt to Chl						<1840 h	
12PBA-008a	Unfoliated Hbl monzodiorite	Hbl-Ttn-Ap-Zc-(Chl-Ep)	undeformed; Chl rims on Hbl; cut by Ep rich veins	1822	5					
12PBA-013a	Foliated Bt-Gt-Opx granodiorite diatexite	Bt-Grt-Opx-Mnz-Zc-Ilm-Pyrr	foliation defined by biotite and moderate qfp shape; matrix partially recrystallized; anhedral Grt-Opx rimmed by Bt	1844	7			2958		t
12PBA-014a	Foliated Bt-Hbl granodiorite	Bt-Hbl-Ap-Mt?	foliation defined by Bt; Hbl is equant; partially recrystallized qfp matrix; unaltered						1827h 1770b	
12PBA-023a	Foliated Bt granodiorite	Bt-Ep-Py-Zc	Kfs porphyroclasts wrapped by Bt and high-strain, mostly recrystallized qfp matrix	2589	3			3003		t
12PBA-027a	Strongly foliated And-Gt pelitic schist	And-Grt-Ms-Bt-Sil-Ilm-(Chl-Ms)	And (4-10 mm; replaced by Ms) and Grt (<2 mm) wrapped by strong Ms-Bt defined foliation; some Bt --> Chl; trace Sil aligned w foliation			1861 1844	7 6			m

Mineral abbreviations from Kretz (1989); qfp = quartz-feldspar

[1]Lithology based on normative chemic composition (if available)

[2]Assemblage not including Kfs-Pl-Qz present in all samples (abbreviations from Kretz, 1989);
note: parentheses = late, secondary; italics = altered; underlined = trace

[4]Zircon ages are interpreted as igneous, except metamorphic zircon denoted with "m" (ages from Davis et al. 2014)

[5]Monazite ages are interpreted as metamorphic (see Table 2)

[6]Nd model ages based on De Paulo model (1981)

[7]Interpreted ^{40}Ar-^{39}Ar cooling ages of hornblende (h) or biotite (b) - see Table 3

[8]Whole-rock chemistry for major elements only (m), or major and trace elements (t)

B. Nd isotopic data

Nd isotopic data are reported in Appendix 2 as epsilon (ε) values and depleted-mantle model ages based on the De Paolo (1981) model. ε_{Nd} values were calculated either for the time of crystallization established by U-Pb zircon results (Davis et al., 2014) or for assumed ages based on geochemical or spatial relationships. The regional distribution of model ages is shown on Figure 5. ε_{Nd} values for each geologic domain show the following variations**:**

(a) Mesoarchean rocks within the Mesoarchean block: +3.7 to + 0.7 for the oldest two samples (3.16 – 3.12 Ga; L033, L038), and -3.0 to -1.3 for two slightly younger samples (L031, L019) with 3.11 and ca. 2.96 Ga ages;

(b) within the Rae craton: -1.7 to +0.3 for three dated ca. 2.6 Ga rocks (L008, L044, P023), and between -2.0 to +1.4 for five undated Rae craton rocks (L007, L025, L027, L028, L029, L042) considered likely to be part of the 2.6 Ga suite on the basis of geographic proximity and geochemical similarities (see below); -12.9 for a 1.84 Ga diatexite with 2.8 – 2.6 Ga zircon inheritance (P013; Davis et al., 2014).

(c) within the 2.5 Ga plutonic suite: -0.2 to +0.3 for three dated ca. 2.5 Ga samples (L015, L023, L025) near the Rae – QMG granitoid belt boundary (Fig. 5); -3.7 Ga for a 2488 Ga alkali feldspar granite (L018a) in the Mesoarchean domain, and – 8.5 to -6.3 for two samples that are interpreted to be 2.5 - 2.35 Ga in age based on geochronological constraints (L020c) or location within the aeromagnetically defined QMG belt (L022);

(d) Thelon tectonic zone: -2.0 to -1.6 for two dated 2.03-1.99 Ga samples (L002, L001) in the western Ttz (Fig. 5); between -8.0 to -4.4 for two samples (L032, L039) interpreted to be ca. 2.0-1.9 Ga based on their young Nd model ages relative to the Mesoarchean crust they intrude (Fig. 5); -0.4 for a ca. 2.6 Ga monzogranite (L003).

These Nd isotopic results indicate that: (a) within the Mesoarchean domain, the two oldest rocks were derived from juvenile sources, with an older crustal component involved in the genesis of younger (3.10 – 2.96 Ga) rocks; (b) 2.6 Ga plutonic rocks in the Rae were derived in part from juvenile sources and in part from recycling of pre-2.6 Ga crust that is younger than that in the Mesoarchean block; (c) 2.5 Ga rocks were derived from juvenile sources along the boundary of the Mesoarchean domain and Rae craton, and from old crust where they occur within the Mesoarchean block; and (d) 2.03 – 1.9 Ga rocks were derived from older crustal sources.

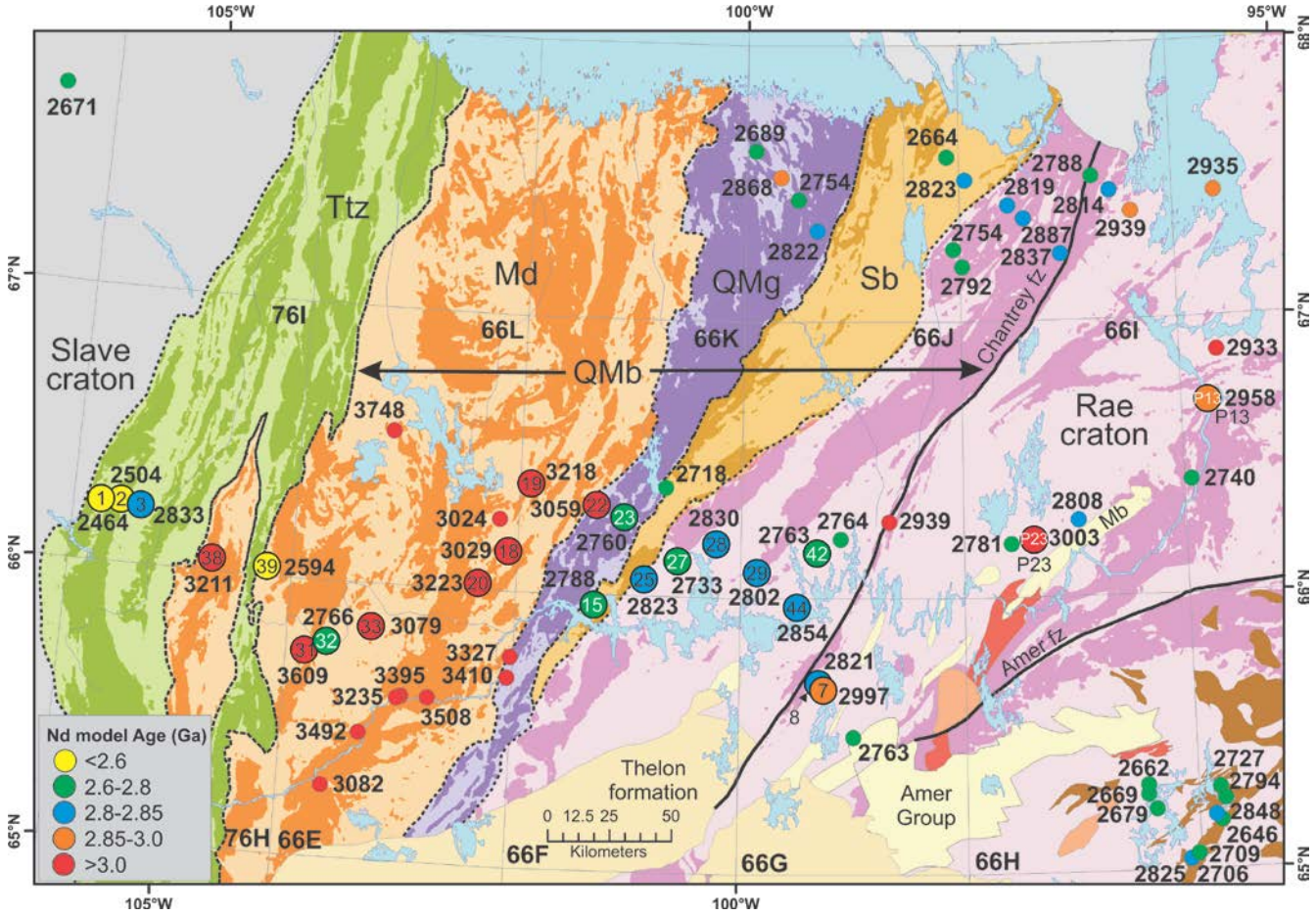

Figure 5. Nd model ages in the Chantrey region. Data from this study are shown as larger symbols with sample numbers. Other data from Theriault et al. (1994), Schultz (2007), Schultz et al. (2007), and compilation of Peterson et al. (2010).

C. Major and trace element geochemistry

Of the 24 rocks analyzed for major and trace elements (Appendices 3a, 3b, 3c), there are an insufficient number of samples in any one crustal domain to establish petrologic trends. Geochemical data for sampled plutonic rocks are shown in Fig. 6 (Q-Anor), which forms the basis for the plutonic rock names used below (see Table 1; Appendix 1). Geochemical data for all samples share a number of characteristics regardless of age and/or crustal domain. All samples have medium to high potassium (Fig. 7), and all except one (L-18b: undated gabbro dyke) are magnesian (Fig 8a). MALI (Na_2O+K_2O-CaO) values are generally more alkalic with decreasing age (e.g. from ca. 3.2 Ga calcic to 2.6 Ga alkali-calcic; Fig. 8b), consistent with an increasing amount of crustal recycling. The more felsic samples of all age groups are peraluminous (Fig. 9), indicating involvement of a sedimentary source in their genesis. Most samples plot in the volcanic arc field on a Rb vs. Y+Nb diagram (Pearce, 1996; Fig. 10), typical of average upper and middle crust. Collectively, the lithogeochemistry suggests that crustal recycling was an important process during the petrogenesis of these rocks.

Within the Thelon tectonic zone, dated samples include 2.03 Ga quartz monzonite (L002) and 1.99 Ga monzogranite (L001), with Nd model ages of ca. 2.5 Ga. Based on the young Nd model ages of samples L032 and L039 in the western Mesoarchean domain (2.77 Ga and 2.59 Ga, respectively), these syenogranite and alkali feldspar granite samples are inferred to be 2.0 – 1.9 Ga in age. If this inference is correct, these four samples display an alkali – calcic trend (Fig. 8). Monzogranite L003, with an upper intercept age of 2591 ± 27 Ma interpreted to date its crystallization (Davis et al., 2014), is tentatively considered part of Slave craton due to its geographic proximity, although it does show geochemical similarities with 2.6 Ga granitoid rocks of the Rae craton discussed below.

Dated 3.2-3.1 Ga samples within the Mesoarchean block include tonalite (L033: 3158±42 Ma), granodiorite (L031: 3108±53 Ma u.i. age), and monzogranite (L038: 3117±21 Ma). The more potassic composition of younger samples, an alkali feldspar granite (L020: <2800 Ma) and syenogranite (L019: 2964±7 Ma), point to crustal recycling (Fig. 7) as a process. As a group, the trace element geochemistry of samples within the Mesoarchean block resemble volcanic arc rocks (e.g. Fig. 10).

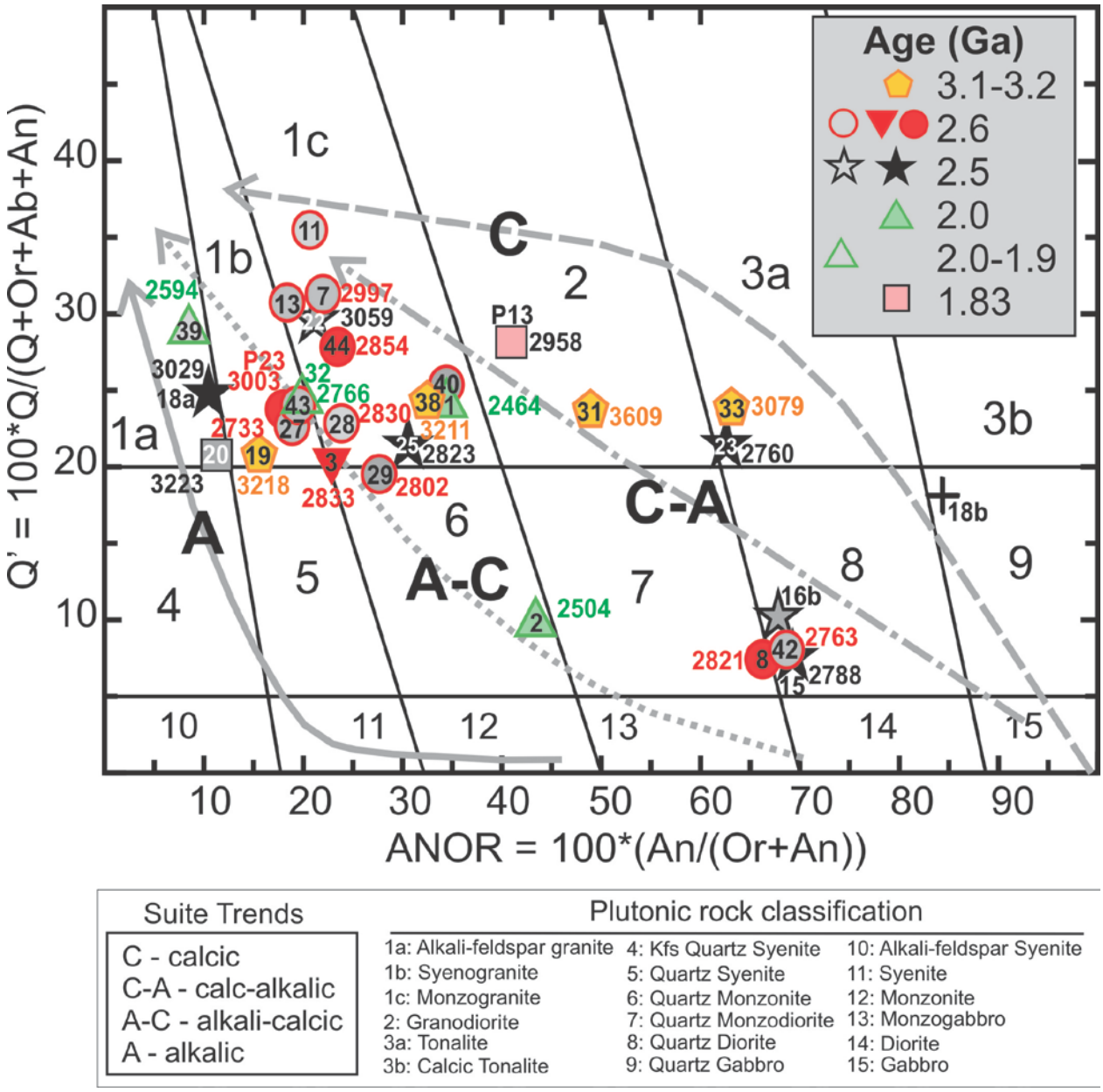

Figure 6. Chantrey area plutonic groups plotted on the CIPW normative Q' (100(Q/(Q+Or+Ab+An)) versus ANOR (100*(An/(Or+An)) classification diagram (Streckeisen and LeMaitre, 1979). Compositional trends for different representative types of plutonic suites (A = alkalic; A-C = alkali-calcic; C-A = calc-alkalic; and C = calcic) are from Whalen and Frost (2013). Legend: colour-filled symbols = U-Pb zircon crystallization ages from Davis et al. (2014); grey-filled symbols = age inferred from location and geochemistry; grey square = sample L20c with 2850 Ma maximum age. Sample numbers are shown mostly inside symbols. Available Nd model ages are shown adjacent to symbols.*

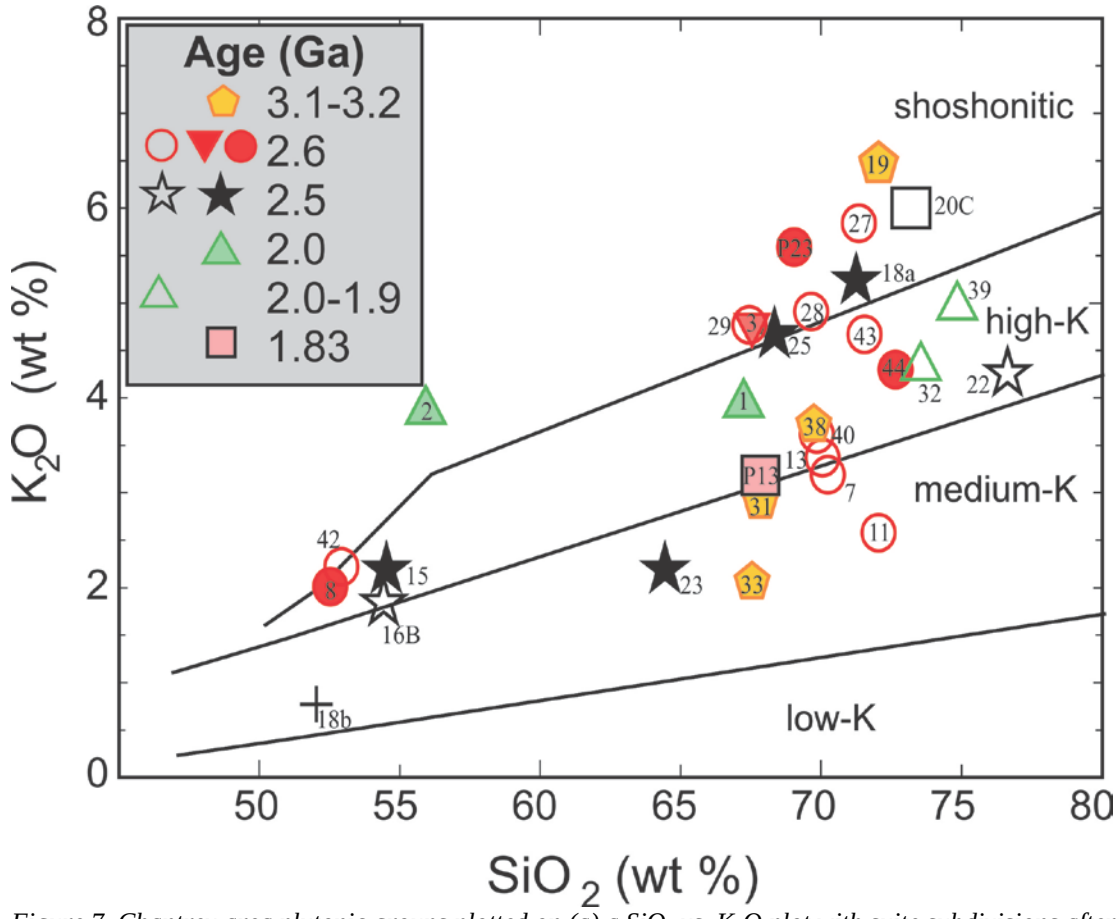

Figure 7. Chantrey area plutonic groups plotted on (a) a SiO_2 vs. K_2O plot with suite subdivisions after LeMaitre (1989) (low-, medium-, high-K) and Peccerillo and Taylor (1976) (high-K, shoshonitic). Sample numbers are shown inside or adjacent to symbols. Open square = sample L20c with 2850 Ma maximum age.

Samples considered part of the 2.5 Ga plutonic suite (Fig. 2, 3) include 2514±3 Ma quartz diorite (L015), undated quartz diorite (L016b), 2524.5±3.5 Ma tonalite (L023), 2506±3 Ma monzogranite (L025), and strongly foliated 2488±5 Ma alkali feldspar granite (L018a). The trace element chemistry of some samples is consistent with a within-plate origin (Fig. 10), but all compositions also fall within the field of post-collisional plutonic rocks.

Samples considered part of the Rae's ca. 2.6 Ga plutonic suite include 2596±3 Ma quartz monzodiorite (L008), undated quartz diorite (L042), 2630±3 Ma (L044) and undated monzogranite (L007, L011, L028, L029, L040), and 2589±3 Ma (P023) and undated syenogranite (L027, L043). As a group they plot between the calc-alkaline and alkali-calcic suite trends (Fig. 8). Although this group of samples plots within the volcanic arc field (Fig. 10), their trend towards potassic compositions (Fig. 7) and the peraluminous nature of most of these rocks (Fig. 9) indicates that crustal melting including a sedimentary source was a significant process in their generation.

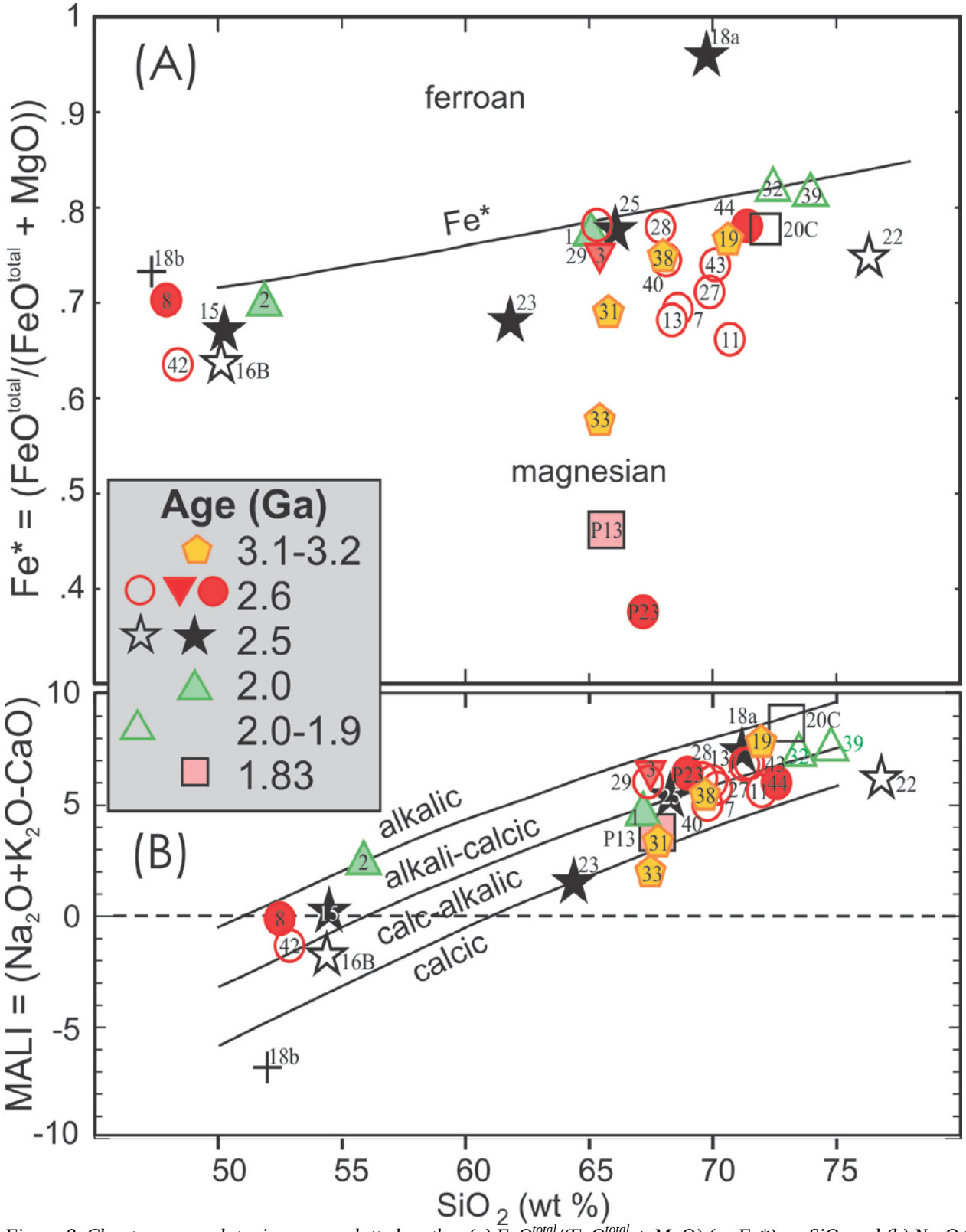

Figure 8. Chantrey area plutonic groups plotted on the: (a) $FeO^{total}/(FeO^{total} + MgO)$ (or Fe) vs. SiO_2 and (b) Na_2O+K_2O-CaO (or MALI) vs. SiO_2 granitic rock classification diagrams of Frost et al. (2001). In (a), the boundary between ferroan and magnesian plutons has been modified, as suggested by Frost and Frost (2008). Symbols as in Figure 7.*

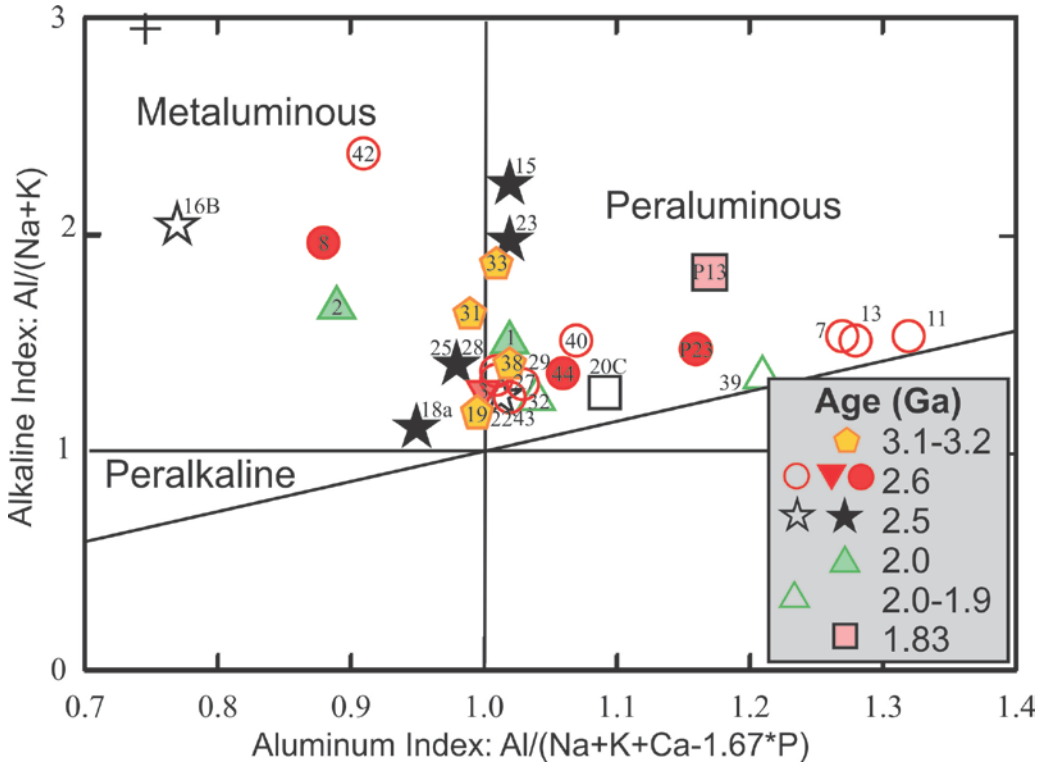

Figure 9: Shad plot of aluminum saturation index versus alkali saturation index modified from Maniar and Piccoli (1989). Symbols as in Figure 7.

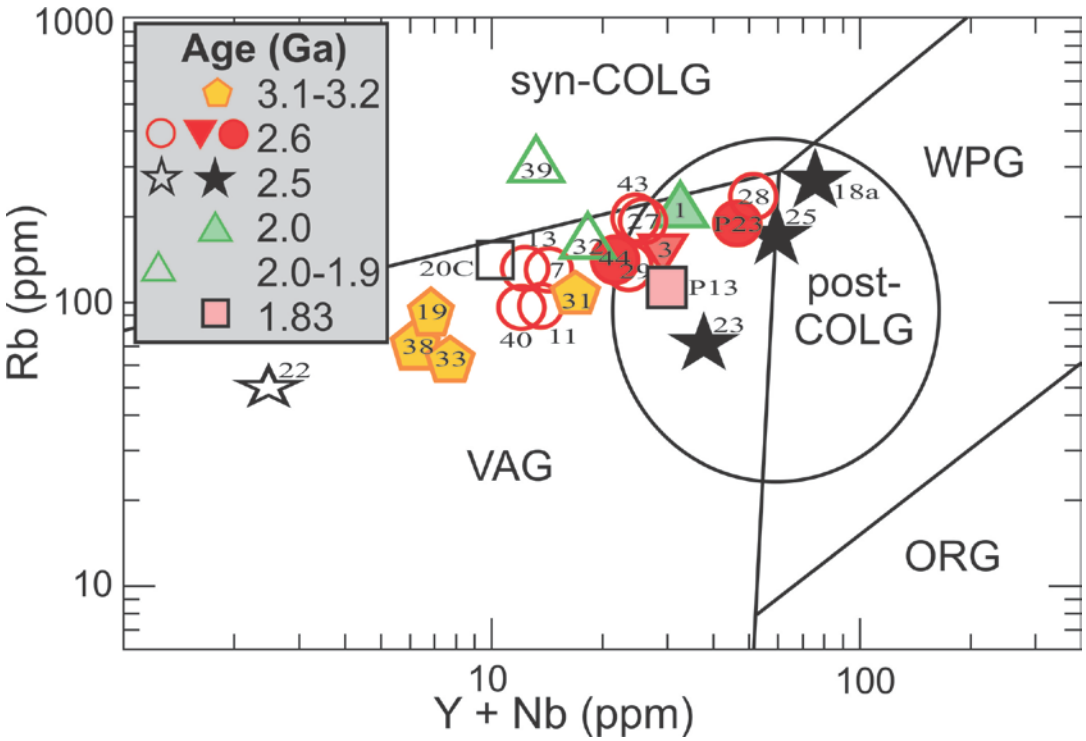

Figure 10. Felsic (>60% SiO_2) Chantrey area plutonic group samples plotted on the Rb-Y+Nb (Pearce, 1996) granitoid tectonic classification diagram. Abbreviations: volcanic-arc (VAG), within-plate (WPG) and syn-collisional (syn-COLG) granitoid fields. Symbols as in Figure 7.

D. Monazite geochronology

U-Pb monazite ages were determined for five samples along the transect (Tables 1; yellow pentagons in Fig. 4): two within the Thelon tectonic zone (L04, L37), one from the eastern Mesoarchean domain (L20), one from the southern end of the Sherman basin (J61), and one from the Montresor belt, Rae craton (P27). Analytical results are provided in Appendices 5a and 5b along with the textural relationships of monazite grains, some of which are shown in Appendix 6. Average age results and related monazite textures are listed in Table 2 and displayed along with regionally available metamorphic ages (van Breemen et al., 1987; Roddick and van Breemen, 1994; Schultz et al., 2007; Tersmette, 2012; Davis et al. 2013, 2014) on Figure 11.

Table 2: *in situ* SHRIMP U-Pb monazite age results

Sample	Age	Error	MSWD	POF	Rock texture or analytical note	Rock texture / monazite location
L-004	**Grt-Sil-Bt metatexite**				Grt-Sil wrapped by recrystallized qfp bands; Bt mostly post-tectonic; Crd-->Chl	
	1992	5	1.4	0.15	oldest 18 spots	Grt inclusions & matrix grains (most aligned with main foliation
	1902	5	1.4	0.11	youngest 19 spots, not including the youngest statistical outlier (32.2)	matrix grains (~50% aligned with main foliation)
	1954	21	0.06	0.8	2 spots on large distinct zone of matrix grain 149, both with highest Th/U over 100	large matrix grain
L-037	**Strongly foliated Grt-Sil diatexite**				small, embayed Grt and Sil in fg, mostly recrystallized qfp matrix; strong foliation defined by alignment of sillimanite and some elongate Grt with attenuated quartz; late Bt from Kfs+Ilm	
	1903	10	2.6	0.001	14 spots on 4 grains, not including grain 9; includes oldest (ca. 1920 Ma) 4 spots (3 grains) since they cannot be distinguished texturally	matrix grains (~50% aligned with main foliation)
	1881	13	1.4	0.24	5 spots on grain 9, which has distinctly lower Th/U = ~18	matrix grain aligned with foliation
JP-061	**Grt-Sil diatexite**				strongly embayed Grt with Sil inclusions & large Kfs porphyroclasts, wrapped by strong foliation defined by qfp shape and Bt and Sil	
	2504	5	1.2	0.3	8 spots on 4 grains, excluding 3 low Y spots in core of patchy-zoned (recrystallized?) grain #43 (analysis 34.1 rejected as statistical outlier)	Grt inclusions & matrix grains aligned with foliation
PBA-027	**Strongly foliated pelitic schist**				And (4-10 mm; replaced by Ms) and Grt (<2 mm) wrapped by strong Ms-Bt defined foliation; some Bt --> Chl; trace Sil aligned w foliation	
	1861	7	1.1	0.34	average of 4 analyses from two grains (54 and 51)	Grt inclusion and matrix grains
	1844	6	0.76	0.64	average of 9 analyses in six grains	Grt inclusion and matrix grains
L-020c	**Grt-Sil S-type granite**				Anhedral, elongate Grt (up to 1 cm long) enveloped by Kfs-rich and Qz-rich layers aligned with scattered Bt blades	
	2367	5	0.071	0.98	4 youngest analyses (3 grains); older analyses (most from Grt inclusions) interpreted as being mixed ages or reset from Archean age	matrix grains aligned with main foliation
L-020a	**Strongly foliated Grt-Bt-Sil diatexite**				Anhedral Grt (up to 6 mm) in part truncates and in part is enveloped by foliation defined by highly attenuated quartz lenses within mostly recrystallized, fg qfp matrix; Sp-Qz intergrowths (after Crd+-Sil?); much Bt is post-tectonic and some from Grt breakdown	
	2369	8	0.31	0.87	5 oldest analyses, all with high Th	Grt inclusions & one matrix grain
	2344	12	0.42	0.66	3 spots on grain 6 with very low Th	matrix grain aligned with main foliation

Ages are in Ma, and errors at 2 sigma
Mineral abbreviations from Kretz (1981); qfp=quartz-feldspar
Sample locations are given in Appendix 1

The main features revealed by these data are:

- metamorphism at ca. 2.5 Ga in the southernmost Sherman basin (sample J61) synchronous with Queen Maud granitoid plutonism (Schultz et al., 2007; Davis et al., 2013, 2014); this sample is interpreted to represent a pre-Sherman basin, Rae margin metasedimentary rock, given that the Sherman basin is constrained to be younger than 2.45 Ga (Schultz et al., 2007)
- metamorphism at ca. 2.35 Ga across the entire 120 km breadth of the central Mesoarchean domain, consistent with that documented across the north by Tersmette (2012);
- an early episode of ca. 2.0 Ga monazite growth in Ttz, roughly synchronous with a major pulse of plutonism (Davis et al., 2014)
- a major metamorphic event at ca. 1.905 Ga across the Ttz and within the western part of the Mesoarchean domain, with a suggestion that it may have extended across the Mesoarchean domain (i.e. sample L25)
- ca. 1.84 Ga metamorphism in the Montresor belt, at much lower grade (lower-amphibolite facies) than similar-aged diatexite further north (sample P13)

E: Thermobarometric data

P-T data were determined for the 5 samples for which monazite ages were obtained, and their main textural features are given in Table 2. Table 3 summarizes mineral compositions of these samples and calculated P-T results. Interpreted ages associated with P-T results (Table 3) are based on the monazite geochronology presented above (Table 2). As tabulated P-T results are based on near-rim compositions, they in general do not represent near-peak P-T conditions. No attempt was made to retrieve P-T conditions from core compositions due to the geochronological evidence in most samples for multiple phases of monazite growth which is assumed to have been associated with recrystallization and re-equilibration of matrix silicate phases. For middle amphibolite-facies sample PBA027, which shows a limited range in monazite ages, the distinctly higher calcium garnet core (Table 3) is interpreted to indicate growth at higher pressure than the tabulated P-T result. Hence this sample records a clockwise P-T-t path.

Table 3. Thermobarometric and mineral compositional data

				Grt				Bt	Crd	Pl	Eqa[c]
Sample	P(kbar)	T(°C)	Age (Ga)[a]	Profile[b]	Fe*	Grs	Sps	Fe*	Fe*	An	
Thelon tectonic zone											
L004	5.3	670	1.91	2.8	76-78	3.0-3.5	1.0-1.2	68->74	73-75	33-37	1,3
L037	4.4	645	1.91	0.6	63-67	2.7-2.9	0.9-1.1	24-25	23-27	31-34	1-5
Mesoarchean block											
L020a	4.6	690	2.35 ?	3,2	68->74	4.0->3.0	1.4-1.8	68->74	-	37	1,3
Sherman basin											
JP061	5.4	640	1.9-1.8	0.75	76->75	2.9->2.2	2.6->1.7	33-37	-	15->36	1,3
Montresor belt (Rae craton)											
PBA027	3.3	575	1.85	1.5	91.5-93	5.8->5.1	6.0-6.1	.71--.69		37->43	1,3,4,7

Average compositions are in mol %, except Fe* = Fe/(Fe+Mg); compositional variations are ±1%
P, T values derived from intersections of listed equilibria (estimated absolute errors are ±50°C, 1 kbar)
[a]Age (Ga): interpreted age of P-T conditions, based on monazite geochronology
[b]Length of core to rim compositional profile (mm)
[c]Eqa: (1) Alm + Phl = Py + Ann; (2) 3 Fcrd + 2 Py = 3 Mg-Crd + 2 Alm; (3) Grs = 3 An + 2 Sil + Qtz;
(4) 3 Eastonite + 6 Qtz + 2 Grs + Py = 3 Phl + 6 An; (5) 3 Fcrd = 2 Alm + 5 Qtz + 4 Sil
(6) Ilm + Py = Alm + Geik; (7) Ms + Gr + Alm = Ann + 3 An
65->76: values show core to rim zonation
71--69: values show change with increasing distance from garnet porphyroblast

F. ^{40}Ar-^{39}Ar geochronology

^{40}Ar-^{39}Ar ages were determined for four samples (Figs. 4, 11): one from the eastern Mesoarchean domain (L18b), one between the Sherman basin and Chantrey fault zone (L29), and two further east in the Rae craton, from the mouth of the Back River (P14) and from the Neoarchean Woodburn supracrustal belt (P4). Data for additional samples are in progress. Analytical results are provided in Appendices 7a-7d. Age results and interpretations are listed in Table 4, with spectra for these four samples shown in Figures 12a-b. Nominal cooling ages for hornblende and biotite are considered to be ca. 500°C and ca. 300˚C, respectively.

Although of a reconnaisance nature, the argon cooling data point to several potential constraints on exhumation and movement on regional-scale faults within the map area. Aliquots 1 and 2 of hornblende from sample L018b in the eastern Mesoarchean domain (Fig. 11) yielded spectra (Fig. 12a) that are saddle-shaped and downward-stepping in age, respectively, patterns which are both indicative of the presence of excess ^{40}Ar. Data plotted on an inverse isochron diagram (not shown) suggest multiple excess Ar compositions are present in the sample and a robust inverse isochron age is not resolvable. As such the interpreted age from the release spectra represents a maximum age only. Thus further investigation of cooling ages in this domain is required to determine whether this region cooled below hornblende closure during the early ca. 2.0 Ga stage of the Thelon orogeny and was not significantly affected by the ca. 1.9 Ga event that is prominent in the Ttz and western Mesoarchean domain (Fig. 11).

The interpreted cooling age for biotite from L29 is 1863 ± 7 Ma, similar to a possible older ca. 1863 Ma monazite population in sample P27 further east (Fig. 11). Accordingly sample L29, located west of the Chantrey fault, may record the western extent of Trans-Hudson orogen-related metamorphism. In contrast, sample P14 to the east of the Chantrey fault (Fig. 11) yielded interpreted hornblende and biotite cooling ages of 1827 ± 11 and 1770 ± 11 Ma, respectively, and a nearby diatexite (P13), yielded a zircon age for crustal melting of 1844±7 Ma. Collectively, these data suggest that the region west of the Chantrey fault was cooling and likely being exhumed, while the region east of the Chantrey fault was being heated. Lastly, sample P4, collected from the Neoarchean Woodburn supracrustal belt located south of the Amer shear zone, yielded an interpreted maximum metamorphic cooling age for hornblende of ca. 1840 Ma. Since ca. 1840-1830 Ma metamorphic monazite ages are recorded nearby in the Woodburn Lake area (Pehrsson et al., 2013), the actual cooling age of hornblende is likely to be somewhat younger.

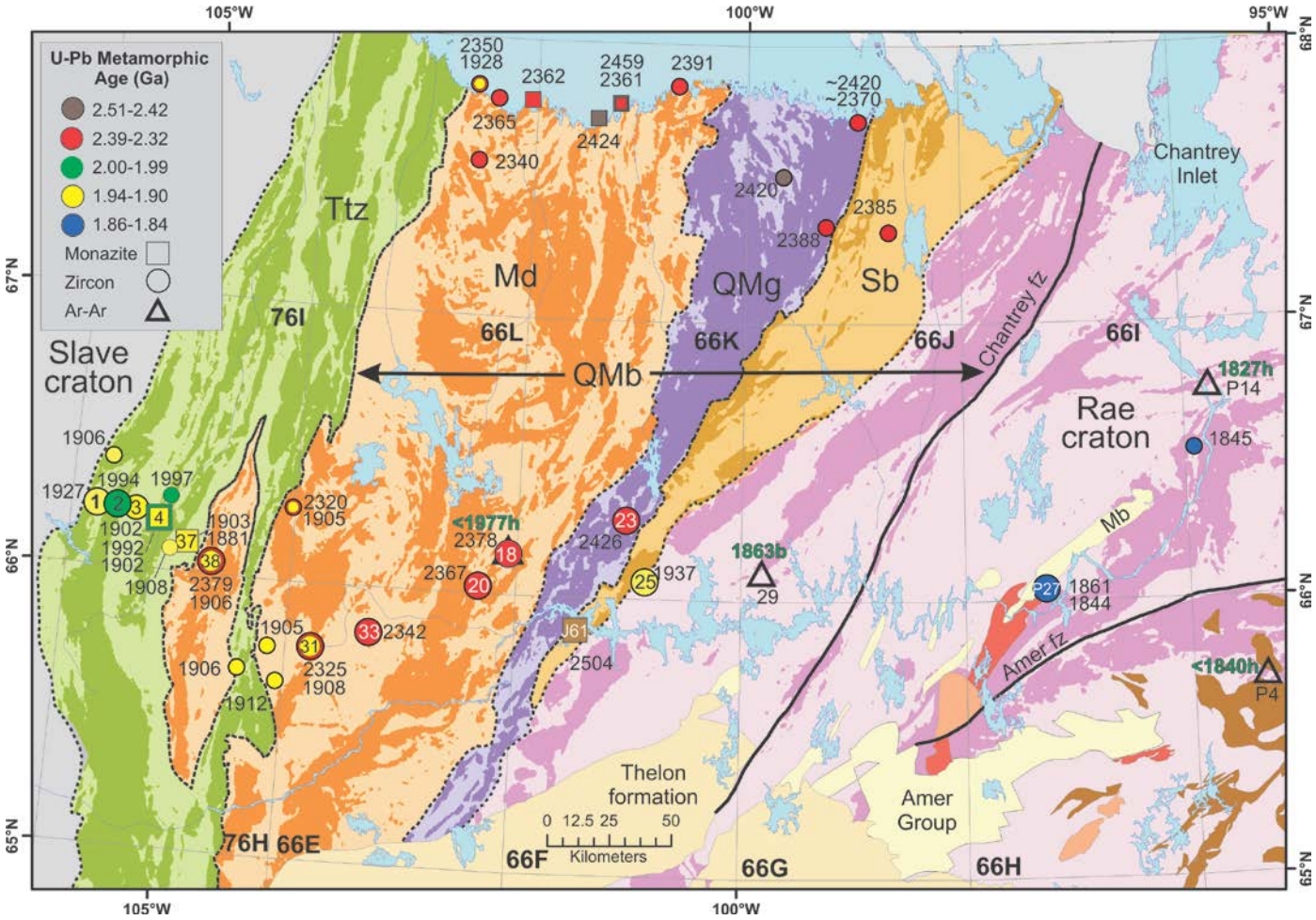

Figure 11. U-Pb metamorphic monazite and ^{40}Ar-^{39}Ar (hornblende = h; biotite = b) ages in the Thelon-Chantrey region. Data with abbreviated sample numbers are from this study and that of Davis et al. (2014). Also shown are data from the northern Sherman basin (Schultz et al., 2007) and from a Queen Maud Gulf coastal transect (Tersmette, 2012).

Table 4: Ar-Ar age results

Sample	Lithology	Min[1]	Age	Error	MSWD	Interpretation	Interpretation notes	Textural notes
12NKL-018b	Undeformed Cpx-Hbl quartz gabbro dyke	Hbl	~1977			max. post-dyke emplacement cooling age	coincidence of youngest portions of step heat spectra for two single crystal aliquots (aliquot 1 steps f-k 1977±10 Ma; aliquot 2 steps f-h,j 1976±9 Ma)	Hbl grains (<0.5mm) & rims on Cpx; minor Hbl->Bt
12NKL-029a	Foliated Hbl-Bt-Mt quartz monzonite	Bt	1863	7	0.7	cooling age (~300C)	plateau ages from two single crystal aliquots with 10 Ma error and MSWD = 2, n = 5,7	Bt (0.5-2 mm long) defines foliation
12PBA-004a	Hbl-Bt tonalite gneiss	Hbl	~1840			maximum metamorphic cooling age	comparison of youngest portions of step heat spectra for three single crystal aliquots: aliquot 1 is youngest at 1841±7 Ma for steps h-o	Hbl (0.4-2 mm) defines foliation; minor Hbl->Bt
12PBA-014a	Foliated Bt-Hbl granodiorite	Hbl	1827	11		metamorphic cooling age (~500C)	no plateau: aliquot 1 steps n-o (>80% total gas) 1827±11 Ma; aliquot 2 steps e-m (100% total gas) 1826±11 Ma	equant Hbl (0.5-1.5 mm); some Hbl->Bt; Bt defines foliation
12PBA-014a	Foliated Bt-Hbl granodiorite	Bt	1770	11	1.5	metamorphic cooling age (~300C)	plateau age from single crystal aliquot, n = 8, steps r-z (87.5% total gas)	

[1]Mineral dated

Ages are in Ma, and errors at 2 sigma

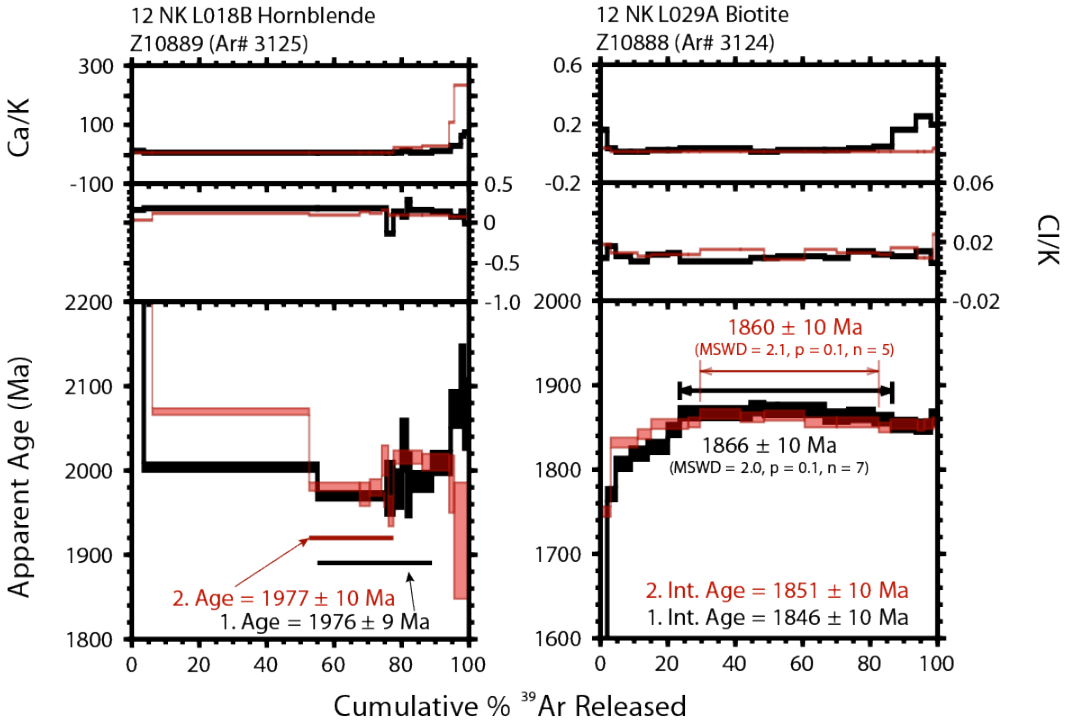

Figure 12a: $^{40}Ar/^{39}Ar$ step heat spectra for samples 12NK L018b (left) and 12NK L029a (right). Analyses represent single-crystal aliquots, with results numbered according to aliquot. Only steps comprising ≥1% total $\%^{39}Ar$ released are plotted and used to calculate ages. "Int Age" represents the integrated age of 100% ^{39}Ar released. "Age" represents a particular set of consecutive age steps of the step heat spectra used to make an age interpretation. Steps used for these calculations are indicated in the figures with a coloured bar and in the data tables by greyed cells. The rationales for the selections are listed in the age summary table. Arrows denote steps that produce a statistical plateau, with statistics reported above the plateau region. Plateau criteria are described in the methods.

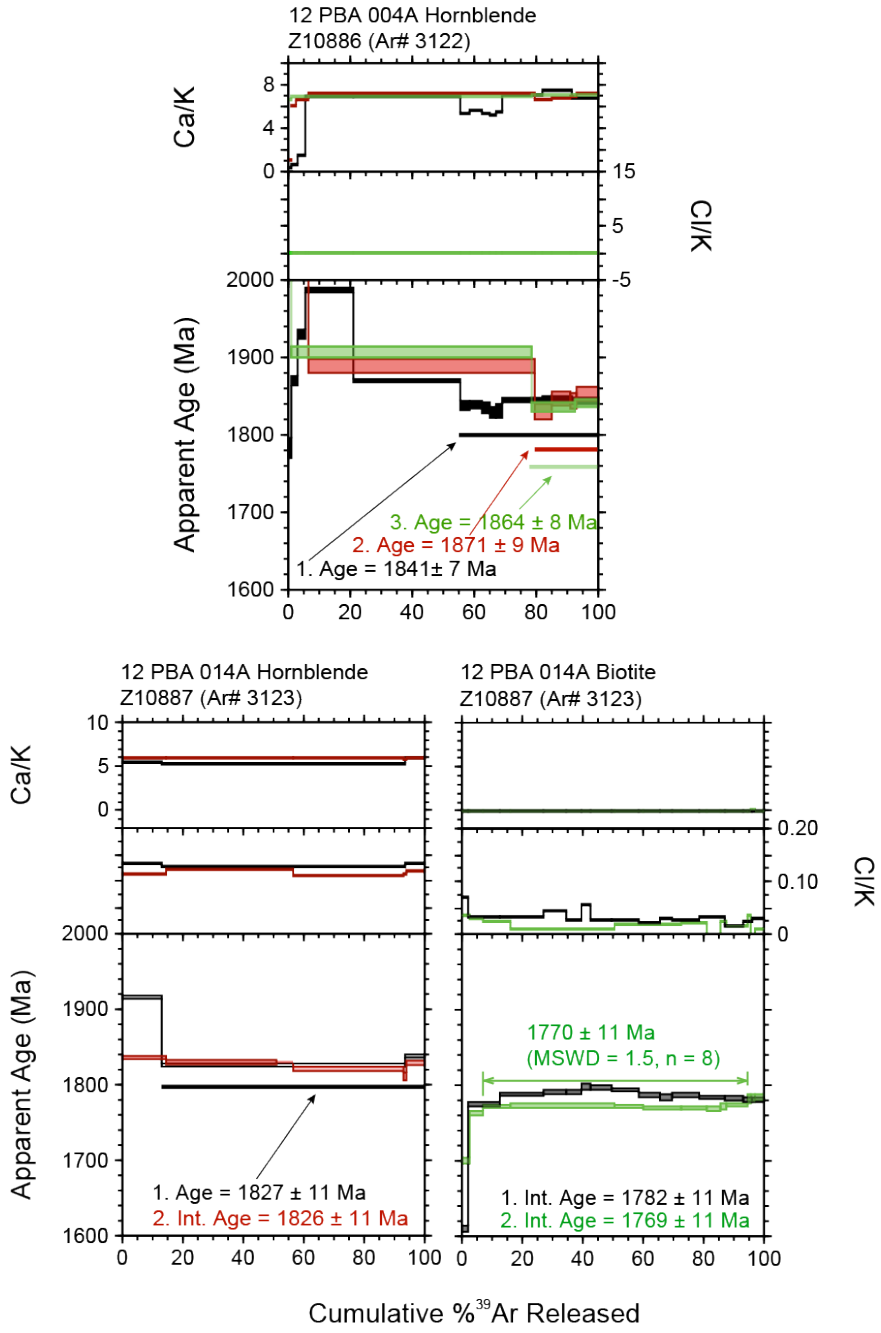

Figure 12b: $^{40}Ar/^{39}Ar$ step heat spectra for samples 12PBA-004a (top) and 12PBA-014a (bottom). See caption of Figure 12a for explanation.

Discussion

The data presented in this report, together with the geochronology of some of these samples (Davis et al., 2014) and from transects further north (Schultz et al., 2007; Tersmette, 2012; Davis et al., 2013) provide a strong basis for division of the Chantrey region into five crustal domains (Figs. 2, 3). The Mesoarchean domain is characterized by Nd model ages between 3.6 – 3.0 Ga (Fig. 5) and U-Pb zircon ages between 3.2 – 3.0 Ga (Fig. 2). This crustal block preserves a record of reworking during formation of the ca. 2.54 – 2.3 Ga Arrowsmith orogen (Berman et al., 2005; 2013b). Whereas ca. 2.5 Ga monazite growth appears spatially associated with ca. 2.5 Ga QMg plutonism. (Fig. 11), the transect data document that ca. 2.35 Ga reworking extended across the width of the Mesoarchean block, including the western outlier.

A prominent feature of the western Rae craton is its voluminous ca. 2.6 Ga plutonism (Fig. 2). Nd isotopic data in this region suggest that older crust north of the Montresor belt is flanked to the west by more juvenile crust (Fig. 5). An intriguing feature of the overall geochronological dataset is the apparent absence of ca. 2.6 Ga plutonism in the adjacent Mesoarchean domain (Fig. 2; Davis et al., 2014), suggesting that it had not accreted to the Rae until after this time. In contrast, ca. 2.5 Ga plutonic rocks are present outside of the main QMg belt, both to the west in the Mesoarchean block and to the east in the Rae craton (Fig. 2; Davis et al., 2014). These constraints suggest that the collision of these blocks occurred after ca. 2.6 Ga and prior to 2.5 Ga, and thus offer some support for the convergent tectonic setting at ca. 2.54 Ga interpreted from monazite dating of deformation fabrics on southern Boothia peninsula and Melville peninsula (Berman et al., 2013b; 2015). A collision between the Mesoarchean block and the Rae may have been accompanied by a subduction zone jump to the west, placing this boundary in a back arc setting that could account for the rift-like geochemical character of QMg plutonism (Schultz et al., 2007, 2010). One problem with this interpretation is the current lack of evidence of an accompanying magmatic arc.

Plutonism in the Thelon tectonic zone is now constrained to have initiated at least as early as 2029 Ma (Davis et al., 2014), some 30 m.y. earlier than previously recognized, and raising the question of whether it is correlative with that in the Taltson magmatic zone (Bostock and van Breemen, 1987), as commonly assumed (Hoffman, 1988). The available data emphasize a major plutonic pulse at ca. 2000 Ma extending along the length of the belt (Fig. 2). This episode also includes granodiorite much further east (Davis et al., 2013), which provides the basis for interpreting that a Thelon-aged plutonic belt intrudes Mesoarchean crust (Figs. 2, 3). While there is some evidence of metamorphism at this time, perhaps reflecting regional contact metamorphism, the most widespread metamorphic event occurred at ca. 1905 Ma (Fig. 2) and appears to have involved widespread S-type granite generation (van Breemen et al., 1987; Davis et al., 2013). This episode of metamorphism is considered to reflect crustal thickening driven by indentation of the Slave craton.

Recognition of ca. 2.6 Ga monzogranite gneiss in the central portion of the Thelon tectonic zone (Fig. 2; Davis et al., 2014) has far-reaching implications. The proximity of the Slave craton with its widespread ca. 2.6

Ga granitoid suite, combined with the apparent absence of this aged plutonism in the Mesoarchean domain, makes it likely that Slave crust underlies this part of the Ttz. However, further work is needed to understand whether this is a result of structural imbrication or whether Thelon plutonism was intracontinental in nature (Thompson, 1989; Schultz et al., 2007). In either scenario, the inferred association of this crust to the Slave craton with its demonstrated economic prospectivity, greatly enhances the economic potential of geochemical anomalies discovered in this region (McCurdy et al., 2013).

U-Pb monazite and $^{40}Ar/^{39}Ar$ hornblende and biotite ages document that Hudsonian reworking extends west across the Chantrey fault zone (Fig. 2). The clockwise P-T-t path and ca. 1.85 Ga age of monazite in basement to the Montresor belt (sample P27) are very similar to the timing and style of metamorphism documented in the Committee Bay belt further east (Fig. 1; Berman et al., 2005, 2010).This tectonic thickening of the central Rae craton has been modelled to have been driven by ca. 1870 Ma collision of Meta Incognita microcontinent with the southeastern flank of the Rae (Berman et al., 2010). Later extensional faulting has been recently proposed (Percival et al., 2014) to have juxtaposed lower grade rocks of the Montresor belt with basement that ranges from middle-amphibolite facies (P27) to upper-amphibolite facies (P14).

Acknowledgements

We gratefully acknowledge the support of Polar Continental Shelf Program and Great Slave Helicopters, as well as K. Venance for microprobe analyses, P. Hunt for SEM imaging, and N. Rayner and T. Pestaj with SHRIMP analyses. M. Sanborn-Barrie provided a very comprehensive and constructive review that helped to improve this report.

References

Ashton, K.E., 1988. Precambrian geology of the southeastern Amer Lake area (66H/1), near Baker Lake, N.W.T.; a study of the Woodburn Lake Group, an Archean orthoquartzite-bearing sequence in the Churchill structural province. Queen's University, Kingston, ON, Canada, Doctoral thesis, 335 p.

Berman, R.G., 2007. winTWQ (version 2.3): A Microsoft Windows-compatible software package for performing internally-consistent thermobarometric calculations; Geological Survey of Canada Open File, v. 5462.

Berman, R.G., Davis, W.J., Corrigan, D., and Nadeau, L., 2015. Insights into the tectonothermal history of Melville Peninsula, Nunavut provided by *in situ* SHRIMP geochronology and thermobarometry; Current Research Geological Survey of Canada (in press).

Berman, R.G., Pehrsson, S., Davis, W.J., Ryan, J., Qiu, H., and Ashton, K.E., 2013b. The Arrowsmith orogeny: new insights from in situ SHRIMP geochronology of the southwestern and central Rae craton; Precambrian Research, v. 232, p. 44-69.

Berman, R.G., Percival, J.A., Harris, J.R., Davis, W.J., McCurdy, M., Normandeau, P., Case, G., Nadeau, L., Hillary, E.M., Girard, E., Jefferson, C.W., Kellett, D., Camacho, A., Bethune, K., Pehrsson, S., and Hunt, P., 2013a. Geo-Mapping Frontiers' Chantrey project: Reconnaissance geology and economic potential of a transect across the Thelon tectonic zone, Queen Maud region, and adjacent Rae craton, Geological Survey of Canada, Open File 7394.

Berman, R.G., Ryan, J.J., Davis, W.J., and Nadeau, L., 2008. Preliminary results of linked in-situ SHRIMP dating and thermobarometry studies in the Boothia mainland area, north-central Rae Province, Nunavut; Current Research Geological Survey of Canada, v. 2008-2, p. 13p.

Berman, R.G., Sanborn-Barrie, M., Stern, R.A., and Carson, C., 2005. Tectonometamorphism at ca. 2.35 and 1.85 Ga in the Rae domain, western Churchill Province, Nunavut, Canada: insights from structural, metamorphic and in situ geochronological analysis of the southwestern Committee Bay belt; Canadian Mineralogist, v. 43, p. 409-442.

Berman, R.G., Sandeman, H.A.I., and Camacho, A., 2010. Diachronous deformation and metamorphism in the Committee Bay belt, Rae Province, Nunavut: insights from ^{40}Ar-^{39}Ar cooling ages and thermal modelling; Journal of Metamorphic Geology, v. 28, p. 439–457.

Bostock, H H; Donaldson, J A; Fraser, J A; Poole, W H; Williams, F M G; Geological Survey of Canada, Preliminary Map 45-1963, 1963; 1 sheet, doi:10.4095/108836

Bostock, H.H., Van Breemen, O., and Loveridge, W.D., 1987. Proterozoic geochronology in the Taltson Magmatic Zone, N.W.T; Geological Survey of Canada, Paper, v. 87-2, p. 73-80.

Chacko, T., De, S.K., Creaser, R.A., and Muehlenbachs, K., 2000, Tectonic setting of the Taltson magmatic zone at 1.9-2.0 Ga: A granitoid-based perspective, Canadian Journal of Earth Sciences, v. 37, p. 1597-1609.

Davis, W., Berman, R.G., and MacKinnon, A., 2013, U-Pb Geochronology of Archival Rock Samples from the Queen Maud Block, Thelon Tectonic Zone and Rae Province, Kitikmeot Region, Nunavut, Canada, Geological Survey of Canada Open File, 7409.

Davis, W., Berman, R.G., Nadeau, L., and Percival, J.A., 2014. U-Pb Geochronology of a transect across the Thelon Tectonic Zone, Queen Maud block, and adjacent Rae craton, Kitikmeot Region, Nunavut, Canada Geological Survey of Canada Open File, 7652.

Deino, A.L., 2001. Users manual for Mass Spec v. 5.02. Berkeley Geochronology Center Special Publication 1a, 119 p.

DePaolo, D.J., 1981. Neodymium isotopes in the Colorado Front Range and crust-mantle evolution in the Proterozoic; Nature, v. 291, p. 193-196.

Fraser, J., 1988. Geology of the Woodburn Lake map area, District of Keewatin; Geological Survey of Canada Paper, v. 87-11, p. 12p.

Frisch, T., 1983. Precambrian geology of the Prince Albert Hills, western Melville Peninsula, northwest territories; Geological Survey of Canada, Bulletin, v. 346, p. 70p.

Frisch, T., 2000. Precambrian geology of Ian Calder Lake, Cape Barclay, and part of Darby Lake map areas, south-central Nunavut; Geological Survey of Canada, Bulletin, v. 542, p. 51.

Frith, R.A., 1982a. Geology, Beechey Lake-Duggan Lake, District of Mackenzie; Geological Survey of Canada, Open File, v. 851 (1:125,000).

Frith, R.A., 1982b. Second preliminary report on the geology of the Beechey Lake-Duggan Lakes map areas, District of Mackenzie, Geological Survey of Canada Paper, v. 82-1A, p. 203-211.

Frith, R.A., and van Breemen, O., 1990. U-Pb zircon age from the Himag plutonic suite, Thelon Tectonic Zone, Churchill Structural Province, Northwest Territories, Geological Survey of Canada, Paper, v. 89-2, p. 49-54.

Frost, B.R., Barnes, C.G., Collins, W.J., Arculus, R.J., Ellis, D.J., and Frost, C.D. 2001. A geochemical classification for granitic rocks. Journal of Petrology, 42: 2033-2048.

Frost, B.R., and Frost, C.D. 2008. A geochemical classification for feldspathic igneous rocks. Journal of Petrology, 49: 1955-1969.

Harris, J.R., Hillary, E.M., Percival, J.A., Buller, G., Buenviaje, R., Bazor, D., Baer, S., Kiessl, G.M., Pehrsson, S.J., Davis, W.J., Berman, R.G., Wodicka, N., Beauchemin, M., Coyne, M., and Therriault, A.M., 2013. Geo-mapping Frontiers: Updated information on the regions covered by Operations Baker, Bathurst, Keewatin, Northern Keewatin, Thelon and Wager; Nunavut and Northwest Territories; Geological Survey of Canada, Open File, 7025.

Henderson, J.B., McGrath, P.H., James, D.T., and Macfie, R.I., 1987, An integrated geological, gravity and magnetic study of the Artillery Lake area and the Thelon tectonic zone, District of Mackenzie, Geological Survey of Canada Paper, v. 87-1A, p. 803-814.

Henderson, J.B., McGrath, P.H., Theriault, R.J., and Van Breemen, O., 1990. Intracratonic indentation of the Archean Slave Province Into the Early Proterozoic Thelon Tectonic Zone of the Churchill Province, northwestern Canadian Shield; Canadian Journal of Earth Sciences, v. 27, p. 1699-1713.

Henderson, J.B., and van Breemen, O., 1992, U-Pb zircon ages from an Archean orthogneiss and a Proterozoic metasedimentary gneiss of the Thelon tectonic zone, District of Mackenzie, Northwest Territories, Geological Survey of Canada Paper, v. 91-02, p. 25-33.

Heywood, W.W., 1961. Geological Notes, northern District of Keewatin; Geological Survey of Canada, Paper, v. 61-18.

Heywood, W.W., and Schau, M., 1978. A subdivision of the northern Churchill structural province; Geological Survey of Canada, Current Research, v. 78-1A, p. 139-143.

Hinchey, A.M., Davis, W.J., Ryan, J.J., and Nadeau, L., 2011. Neoarchean high-potassium granites of the Boothia mainland area, Rae domain, Churchill Province: U-Pb zircon and Sm-Nd whole rock isotopic constraints; Canadian Journal of Earth Sciences, v. 48, p. 247-279.

Hoffman, P.F., 1988, United plates of America, the birth of a craton: Early Proterozoic assembly and growth of Laurentia, Annual Reviews in Earth and Planetary Science,, v. 16, p. 543– 603.

Hoffman, P.F., 1989. Precambrian geology and tectonic history of North America; *in* Bally, A.W., and Palmer, A.R. eds.), The geology of North America; an overview: Boulder, CO, Geological Society of America, p. 447-512.

James, D.T., van Breemen, O., and Loveridge, W.D., 1988, Early Proterozoic U-Pb zircon ages for granitoid rocks from the Moraine Lake transect, Thelon Tectonic Zone, District of Mackenzie, Geological Survey of Canada Paper, v. 88-2, p. 67-72.

Jourdan F., Verati, C., Féraud, G. 2006. Intercalibration of the Hb3gr $^{40}Ar/^{39}Ar$ dating standard. Chemical Geology v. 231, p. 177-189.

Kellett, D. and Joyce, N. 2014. Single- and multi-collection $^{40}Ar/^{39}Ar$ measurements for conventional step-heating and total fusion age calculation using the Nu Noblesse at the Geological Survey of Canada: analytical details. Technical Note, Geological Survey of Canada publication, v. 8, 27 pp. doi: 10.4095/293465.

LeMaitre, R.W., 1989. A Classification of Igneous Rocks and Glossary of Terms. Oxford: Blackwell, 193pp.

Maniar, P.D., Piccoli, P.M., 1989. Tectonic discrimination of granitoids. Geol. Soc. Amer. Bull., v. 101, p. 635–643.

McMartin, I., Normandeau, P., Berman, R.G., and Percival, J., 2013, Geo-Mapping Frontiers' Chantrey project: Till geochemistry and mineral/clast counts of a transect across the Thelon tectonic zone, Queen Maud block, and adjacent Rae craton, Geological Survey of Canada Open File, 7418.

McCurdy, M.W., Berman, R.G., Kerr, D.E., and Vaive, J.E., 2013. Geochemical, Mineralogical and Kimberlite Indicator Mineral Data for Silts, Heavy Mineral Concentrates and Waters, Duggan Lake Area, Nunavut (NTS 76H and 76I South); Geological Survey of Canada, Open File, 7471.

MacHattie, T. 2008. Geochemistry and geochronology of the late Archean Prince Albert group (PAg), Nunavut, Canada. PhD thesis, University of Alberta, 340pp.

Natural Resources Canada, 2013. Geoscience Data Repository: Aeromagnetic Data. On-line data from http://gdrdap.agg.nrcan.gc.ca/geodap/index_e.html.

Pearce, J.A., 1996. Sources and settings of granitic rocks. Episodes, v. 19, p. 120-125.

Pearce, J.A., Harris, N.B.W., and Tindle, A.G. 1984. Trace element discrimination diagrams for the tectonic interpretation of granitic rocks. Journal of Petrology, v. 25, p. 956-983.

Peccerillo, A., Taylor, S.R., 1976. Geochemistry of the Eocene calc-alkaline volcanic rocks from Kastamonu area, northern Turkey. Contributions to Mineralogy and Petrology, v. 58, p. 63-81.

Pehrsson, S., Berman, R.G., and Davis, W.J., 2013. Paleoproterozoic orogenesis during Nuna aggregation: a case study of reworking of the Archean Rae craton, Woodburn Lake, Nunavut; Precambrian Research, v. 232, p. 167-188.

Percival, J.A., Tschirhart, V., Ford, A., and Dziawa, C., 2014. Report of activities for the Geology and Mineral Potential of the Chantrey-Thelon Area: GEM-2 Montresor project. Geological Survey of Canada, Open File, 7707.

Peterson, T.D., Pehrsson, S., Skulski, T., and Sandeman, H., 2010. Compilation of Sm-Nd isotope analyses of igneous suites, western Churchill Province; Geological Survey of Canada Open File, v. 6439, p. 18p.

Rainbird, R.H., Davis, W.J., Pehrsson, S.J., Wodicka, N., Rayner, N., and Skulski, T., 2010. Early Paleoproterozoic supracrustal assemblages of the Rae Domain, Nunavut, Canada; intracratonic basin development during supercontinent break-up and assembly; Precambrian Research, v. 181, p. 167-186.

Rayner, N. and Stern, R.A., 2002. Improved sample preparation method for SHRIMP analysis of delicate mineral grains exposed in thin sections. Geological Survey of Canada Current. Research, v. 2002-F10, 3p.

Richard, P., N. Shimizu, and C. J. Allègre, 1976. $^{143}Nd/^{146}Nd$, a natural tracer: an application to oceanic basalts, Earth Planet. Sci. Lett., 31, 269-278.

Roddick, J.C., and van Breemen, O., 1994, U-Pb zircon dating; a comparison of ion microprobe and single grain conventional analyses, Current Research of the Geological Survey of Canada, v. 1994-F, p. 1-9.

Sanborn-Barrie, M., Davis, W.J., Berman, R.G., Rayner, N., Skulski, T. and Sandeman, H., 2014. Neoarchean continental crust formation and Paleoproterozoic deformation of the central Rae craton, Committee Bay belt, Nunavut. Canadian Journal of Earth Sciences, *v.* 51(6), p. 635-667.

Schultz, M.E.J., 2007. Queen Maud block, Nunavut - Genesis of a large felsic igneous province in the earliest Paleoproterozoic and implications for Laurentian geotectonic models, M. SC. Thesis, University of Alberta, Edmonton. 71 p.

Schultz, M., Chacko, T., Heaman, L.M., Sandeman, H., and Creaser, R.A., 2010. 2.46 to 2.50 Ga Magmatism in the Queen Maud Block, northern Canada: An early phase of the Arrowsmith Orogeny or a separate rifting event preceding orogeny? Geological Association of Canada - Mineralogical Association of Canada Program with Abstracts, v. 33.

Schultz, M.E.J., Chacko, T., Heaman, L.M., Sandeman, H.A., Simonetti, A., and Creaser, R.A., 2007, Queen Maud block: A newly recognized Paleoproterozoic (2.4-2.5 Ga) terrane in northwest Laurentia, Geology, v. 35, p. 707-710.

Skulski, T., Sanborn-Barrie, M., and Sandeman, H., 2003. Geology, Walker Lake and Arrowsmith River area, Nunavut; Geological Survey of Canada, Open File, 3777.

Stern, R.A., 1997. The GSC Sensitive High Resolution Ion Microprobe (SHRIMP): analytical techniques of zircon U-Th-Pb age determinations and performance evaluation. Geological Survey of Canada Current Research, v. 1997-F, 31p.

Stern, R.A. and Berman, R.G., 2000. Monazite U-Pb and Th-Pb geochronology by ion microprobe, with an application to *in situ* dating of an Archean metasedimentary rock. Chemical Geology, v. 172, p. 113–130.

Streckeisen, A.L., and Le Maitre, R.W. 1979. A chemical approximation to the modal QAPF classification of volcanic province. Neues Jahrbuch fuer Mineralogie. Abhandlungen, v. 136, p. 169-206.

Sun, S.-S, McDonough, W.F., 1989. Chemical and isotopic systematics of oceanic basalt: implications for mantle composition and processes. In: Saunders, A.D., Norry, M.J. (Eds.), Magmatism in the Ocean Basins. Geol. Soc. Spec. Publ. 42, 313–345.

Tella, S., 1994. Geology, Amer Lake (66H), Deep Rose Lake (66G) and parts of Pelly Lake (66F), Geological Survey of Canada, Open File, Volume 1:250000 Report Number 2969.

Tella, S; Heywood, W W, 1978. The structural history of the Amer Mylonite zone, Churchill Structural Province, District of Keewatin. Geological Survey of Canada, Paper no. 78-1C, p. 79-88

Tersmette, D., 2012, Geology, geochronology, thermobarometry, and tectonic evolution of the Queen Maud block, Churchill craton, Nunavut, Canada. M.Sc. thesis: Edmonton, Alberta, University of Alberta, 165 pp.

Thériault, R.J., 1992. Nd isotopic evolution of the Taltson magmatic zone, Northwest Territories, Canada; insights into early Proterozoic accretion along the western margin of the Churchill Province; Journal of Geology, v. 100, p. 465-475.

Thériault, R.J., Henderson, J.B., and Roscoe, S.M., 1994. Nd isotopic evidence for early to mid-Archean crust from high grade gneisses in the Queen Maud Block and south of the McDonald Fault, western Churchill Province, Northwest Territories. *in*: Radiogenic age and isotopic studies, report 8.; Geological Survey of Canada, Current Research, v. 1994-F, p. 37-42.

Thompson, P., 1986. Geology, Tinney Hills-Overby Lake (West Half), District of Mackenzie, Northwest Territories; Geological Survey of Canada, Open File, v. 1316 (1:125,000).

Thompson, P.H., 1989. An empirical model for metamorphic evolution of the Archaean Slave Province and adjacent Thelon Tectonic Zone, north-western Canadian Shield; *in* Daly, J.S., Cliff, R.A., & Yardley, B.W.D. (ed.), Evolution of Metamorphic Belts, Volume 43, Geological Society Special Publication, p. 245-263.

Thompson, P.H., Culshaw, N., Buchanan, J.R., and Manojlovic, P., 1986, Geology of the Slave Province and Thelon tectonic zone in the Tinney Hills-Overby Lake (west half) map area, District of Mackenzie, Geological Survey of Canada Paper, v. 86-1A, p. 275-289.

Van Breemen, O., Hanmer, S.K., and Parrish, R.R., 1990. Archean and Proterozoic mylonites along the southeastern margin of the Slave structural province, Northwest Territories; Geological Survey of Canada Paper, v. 89-2, p. 55-61.

van Breemen, O., and Henderson, J.B., 1988, U-Pb zircon and monazite ages from the eastern Slave Province and Thelon Tectonic Zone, Artillery Lake area, N.W.T, Geological Survey of Canada, Paper, v. 88-2, p. 73-83.

van Breemen, O., Henderson, J.B., Loveridge, W.D., and Thompson, P.H., 1987a. U-Pb zircon and monazite geochronology and zircon morphology of granulites and granite from the Thelon Tectonic Zone, Healey Lake and Artillery Lake map areas, N.W.T., Geological Survey of Canada Paper, v. 87-1A, p. 783-801.

van Breemen, O., Thompson, P.H., Hunt, P.A., and Culshaw, N. 1987b. U - Pb zircon and monazite geochronology from the northern Thelon tectonic zone, District of Mackenzie. Geological Survey of Canada, Paper, v. 87-2, p. 81-93.

Whalen, J.B., and Frost, C.D. 2013. The Q-ANOR diagram: A tool for the petrogenetic and tectonomagmatic characterization of granitic suites. South-Central Section, Geological Society of America, Austin, Texas, abstract.

Wodicka, N., Corrigan, D., Nadeau, L., and Erdmann, S., 2011. New U-Pb geochronological results from Melville Peninsula: unravelling the Archean and Early Paleoproterozoic magmatic history of the north-central Rae craton; Geological Association of Canada - Mineralogical Association of Canada Program with Abstracts, v. 36, p. 236.

Zaleski, E., Pehrsson, S., Duke, N., Davis, W.J., L'Heureux, R., Greiner, E., Kerswill, J.A., 2000. Quartzite sequences and their relationships, Woodburn Lake group, western Churchill Province, Nunavut. Geological Survey of Canada Paper 2000-C7, 10 *pp.*